

GTP release-selective agonists prolong opioid analgesic efficacy

<https://doi.org/10.1038/s41586-025-09880-5>

Received: 2 April 2025

Accepted: 6 November 2025

Published online: 17 December 2025

Open access

 Check for updates

Edward L. Stahl¹✉, Matthew A. Swanson^{1,2}, Vuong Q. Dang³, Michael D. Cameron³, Nicole M. Kennedy³, Thomas D. Bannister³ & Laura M. Bohn^{1,2}✉

G-protein-coupled receptors act as guanine nucleotide exchange factors (GEFs) and facilitate the activation of heterotrimeric G proteins by exchanging GDP for GTP¹. This exchange function is not unidirectional². Here we demonstrate that an agonist can show selective affinity for an active state that prefers the release of GTP. Specifically, for the mu opioid receptor, we show that several agonists have state-selective affinities for promoting GTP release versus GTP binding. We identify two agonists that show a marked preference for promoting release. In mice, marginally efficacious doses of the release-preferring agonist enhance and prolong the antinociceptive effects of morphine and fentanyl without enhancing the respiratory and cardiac effects of fentanyl. Although these observations are limited to simple measures of thermal nociception, they may point to a way to bifurcate physiological responses to such agonists. We propose that the active-state selectivity of an agonist may determine the preferred direction of the receptor GEF function, which may affect the kinetics and selectivity of the engagement of the receptor with downstream effectors; this may ultimately present a means to disentangle multifaceted drug-induced physiological responses.

Heterotrimeric G proteins transduce information to intracellular partners by modulating GTP binding and hydrolysis³. Through their interaction with G-protein-coupled receptors (GPCRs) and effectors, G proteins provide the transducer function that is necessary for the conveyance of extracellular information^{4,5}. Heterotrimeric G proteins consist of an α subunit bound to a β and γ subunit dimer; they remain a trimer while the α subunit is bound to GDP⁶. Receptors provide the transmembrane conduit for a signal between the extracellular agonist and the intracellular G-protein transducer⁷. Specifically, GPCRs undergo a conformational change that acts to catalyse a reaction between the receptor and the $\text{G}\alpha$ protein^{8–10}. This interaction shifts the affinity for $\text{G}\alpha$ binding to GDP to conditions that favour GDP release and GTP binding³. Thus, the receptor acts as a GEF and this reaction is considered to be primarily unidirectional¹¹ (Fig. 1a). However, there have been observations that the GTP loading function of the receptor is reversible—that is, the receptor may facilitate the release of GTP from $\text{G}\alpha$. Early examples of this reversible interaction used nonhydrolysable forms of GTP such as GTP γ S^{3,12}, wherein the dissociation of radiolabelled GTP γ S could be observed upon agonist binding to the receptor. One such study examined the kinetics of the release of ^{35}S -GTP γ S in cells expressing the mu opioid receptor (MOR) and found that the rate of release of nucleotide was increased as a function of a single saturating concentration of agonist and that partial and full agonists maintained their rank order efficacy in both exchange reactions¹³ (^{35}S -GTP γ S binding and ^{35}S -GTP γ S release).

Here we investigate the significance of the release mechanism as a function of agonist concentration and how it can influence drug

responsiveness in vivo. In a linked Article¹⁴, we present extensive pharmacological and biochemical characterizations of the release reaction, which we summarize in the three-state coupling model (Fig. 1a). In the study, we show that the GTP-release function of the receptor adheres to the pharmacological principles that pertain to the GTP-binding function of the receptor. In summary, the release function is dependent on agonist concentration and can be reversed by antagonists, and competitive interactions are preserved between orthosteric agonists and antagonists. Moreover, we demonstrate that the effect is due to activation of the receptor population and not merely a function of receptor occupancy. We provide experimental evidence and a functional state model that establishes that the efficacy and potency of an agonist to promote GTP release can differ from its efficacy and potency to induce GTP binding. Therefore, an agonist may demonstrate selectivity for affecting the equilibrium of the functional active state of the G protein and can show a preference for one state over the other. We also provide evidence that an agonist may have a different rank order potency and efficacy for the two states of the exchange function of a GPCR.

In the present study we show that agonists can induce both GTP binding and GTP release from $\text{G}\alpha$ in a concentration-dependent manner, and that this can be observed for several different GPCRs (Fig. 1). GTP binding is assessed using a conventional method that entails incubating isolated cell membranes in the presence of ^{35}S -GTP γ S and increasing concentrations of agonists^{15,16}. To observe GTP release, we use a ‘pulse-chase’ paradigm, which entails first loading the membrane preparations with ^{35}S -GTP γ S. Since many GPCRs are negatively regulated

¹Department of Molecular Pharmacology and Physiology, Morsani College of Medicine, University of South Florida, Tampa, FL, USA. ²The Skaggs Graduate School of Chemical and Biological Sciences at Scripps Research, La Jolla, CA, USA. ³Department of Molecular Medicine, The Herbert Wertheim UF Scripps Institute for Biomedical Innovation and Technology, Jupiter, FL, USA. [✉]e-mail: EStahl@usf.edu; LBohn@usf.edu

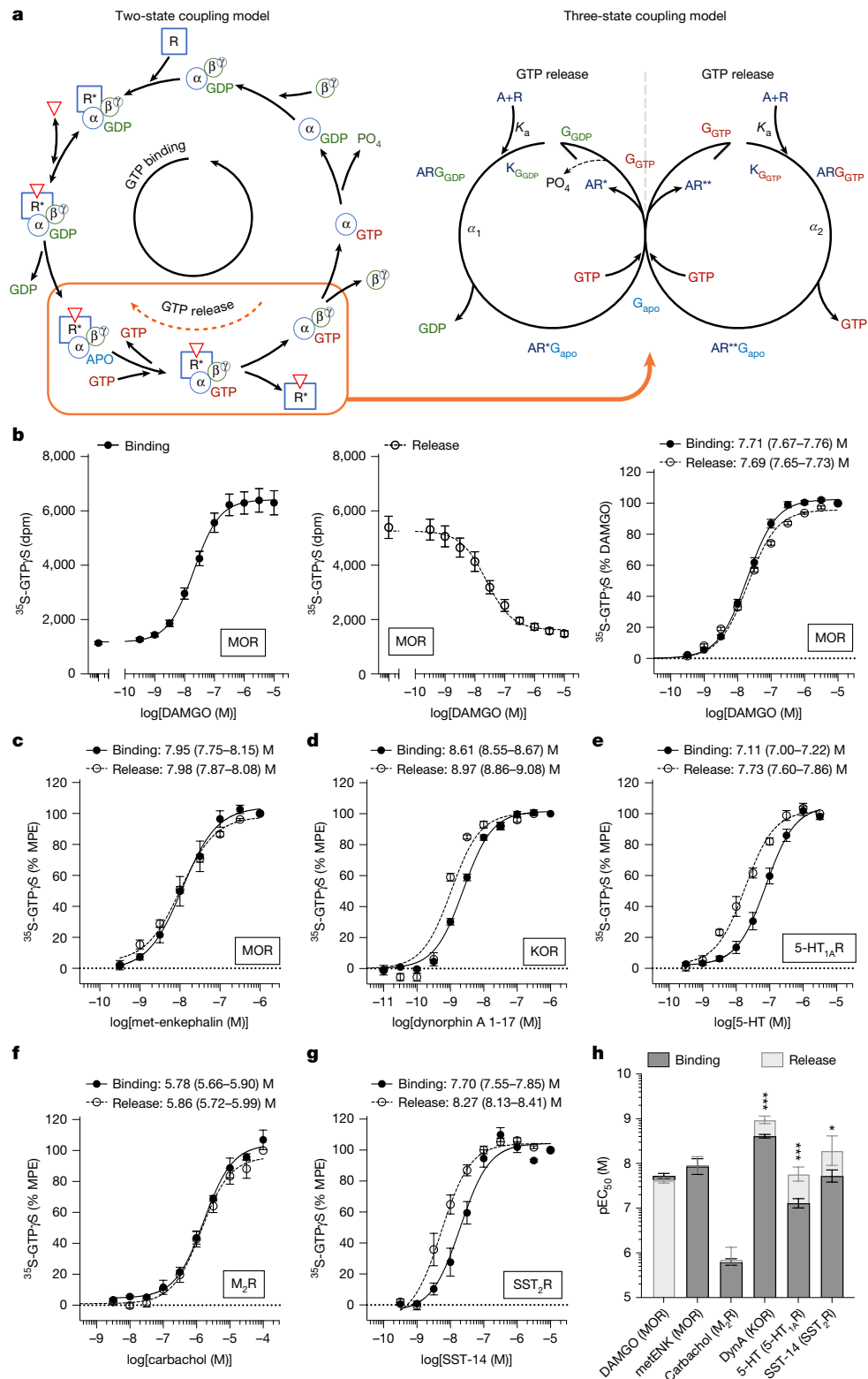


Fig. 1 | GPCRs induce both GTP binding and GTP release from G α proteins and the process is agonist-mediated. **a**, Schematic of the proposed model, showing the conventional pathway of GDP-to-GTP exchange (left) and the expanded model to allow for both GTP and GDP release (right) as detailed in the linked Article¹⁴. A, agonist; R, receptor (asterisks indicate different active states); K_a , affinity constant; G protein; G_{apo}, unbound G protein (blue); G_{GDP}, GDP-bound G protein (green); G_{GTP}, GTP-bound G protein (red); α_1 and α_2 , active state affinities. **b**, DAMGO-stimulated binding and release in CHO-MOR cells presented as raw data (in disintegrations per minute (dpm)) and the normalization to baseline and maximum response. **c–g**, Normalized binding

and release with indicated agonists in CHO-K1 cells expressing MOR (**c**; $n=3$ binding, 3 release), KOR (**d**; $n=3$ binding, 5 release), 5-HT_{1A}R (**e**; $n=8$ binding, 7 release), M₂R (**f**; $n=3$ binding, 3 release) and SST₂R (**g**; $n=4$ binding, 4 release). The raw data are presented in Extended Data Fig. 1. MPE, maximum possible effect. **b–g**, Data are mean \pm s.e.m. and potency is presented as mean with 95% confidence interval. **h**, Comparison of potency in ³⁵S-GTPyS binding versus release by unpaired, two-tailed *t*-test for each receptor comparing the individual potency (pEC₅₀, where EC₅₀ is half-maximal effective concentration) values measured per experiment. Data are mean with 95% confidence interval. * $P < 0.05$, ** $P < 0.01$, *** $P < 0.001$, **** $P < 0.0001$; NS, not significant ($P > 0.05$).

by sodium ions, removal of sodium allows for the constitutive activation of all sensitive receptors and the subsequent loading of ^{35}S -GTPyS binding to G proteins. After the pulse, the chase entails dilution of the membranes and inclusion of an excess of unlabelled (cold) GTPyS in the presence of sodium (see Methods).

The two reactions are compared in Fig. 1b using membranes prepared from cells overexpressing mouse MOR. The data are presented as radioactivity counts for both the binding and the release assay; to facilitate comparison of the potencies, the data are also normalized to the baseline (0%) and the highest concentration used in each response (100%), and the curve is inverted for the release function. For the MOR, the potency of DAMGO ([D-Ala₂, N-MePhe₄, Gly-ol]-enkephalin), an enkephalin analogue, is conserved for both assays and the same is true for met-enkephalin (Fig. 1c). The exchange effect can also be observed for dynorphin A (1–17) at the kappa opioid receptor (KOR), serotonin (5-HT) at the serotonin 1A receptor (5-HT_{1A}R), carbachol at the muscarinic 2 receptor (M₂R) and somatostatin-14 (SST-14) at the somatostatin 2 receptor (SST₂R) (Fig. 1d–g). Notably, agonist potencies at MOR and M₂R are conserved in the two states, whereas dynorphin, serotonin and somatostatin are significantly more potent at their cognate receptors for promoting the release of GTP (Fig. 1h; individual curves are shown in Extended Data Fig. 1).

There are multiple clinically relevant opioid agonists that span a broad range of pharmacological characteristics (including partial agonists and biased agonists); therefore, we used these tool compounds to determine whether the release function and binding function could be dissociated at the MOR. In addition, we tested two new compounds, which were selected on the basis of their scaffold variation from biased MOR agonists introduced by our laboratory (the SR series—for example, SR-17018) and for their characteristics as full agonists that are less potent than morphine in cellular assays. The latter consideration was based on a desire to not introduce more potent opioid agonists to the scientific literature. For each drug, DAMGO was assayed in parallel to serve as a reference, since DAMGO maintains the same potency in both responses and serves to define the maximum efficacy in both assays in this cell line. Not unexpectedly, several agonists perform similarly to DAMGO, preserving the potency in both responses; however, some agonists show a differential preference for potency (Fig. 2a) and/or efficacy (Fig. 2b) for one state over the other (see Extended Data Fig. 2 for curves and Extended Data Table 1 for parameters). Since the two effects were measured in parallel with DAMGO, we also determined the difference in transduction efficiencies ($\Delta\Delta\log R$; Fig. 2c and Extended Data Table 1) for each agonist in the release assay and the binding assay. This representation permits normalization between responses to directly compare agonist activity¹⁷. The two new agonists show significant gains in the release function, having nearly a hundred-fold gain in selectivity for the release active state, as measured by the difference in transduction efficiencies; we have named these compounds muzepan1 and muzepan2 (Fig. 2d), as they are mu opioid receptor-acting compounds containing an 'azepane' ring.

Several of the agonists that show a state preference have previously been identified as biased agonists that prefer G-protein signalling over β -arrestin2 recruitment (for example, oliceridine¹⁸, PZM21¹⁹, herkinorin²⁰, buprenorphine^{21–23} and SR-17018²⁴). When tested in the cellular assays expressing the human MOR that were used to evaluate the biased agonism of SR-17018²⁴, both muzepan1 and muzepan2 show no preference between GTPyS binding and β -arrestin2 recruitment (Extended Data Fig. 3a and Extended Data Table 2). Moreover, the exchange selectivity for GTP release over binding is maintained at the human receptor (Extended Data Fig. 3b, Extended Data Table 3). Therefore, whereas many of the compounds that showed selectivity for release over binding also show preference for G-protein binding over β -arrestin2 recruitment, the correlation is not absolute.

To demonstrate the physiological significance of agonist-induced GTP release, the experiment was repeated in mouse spinal cord

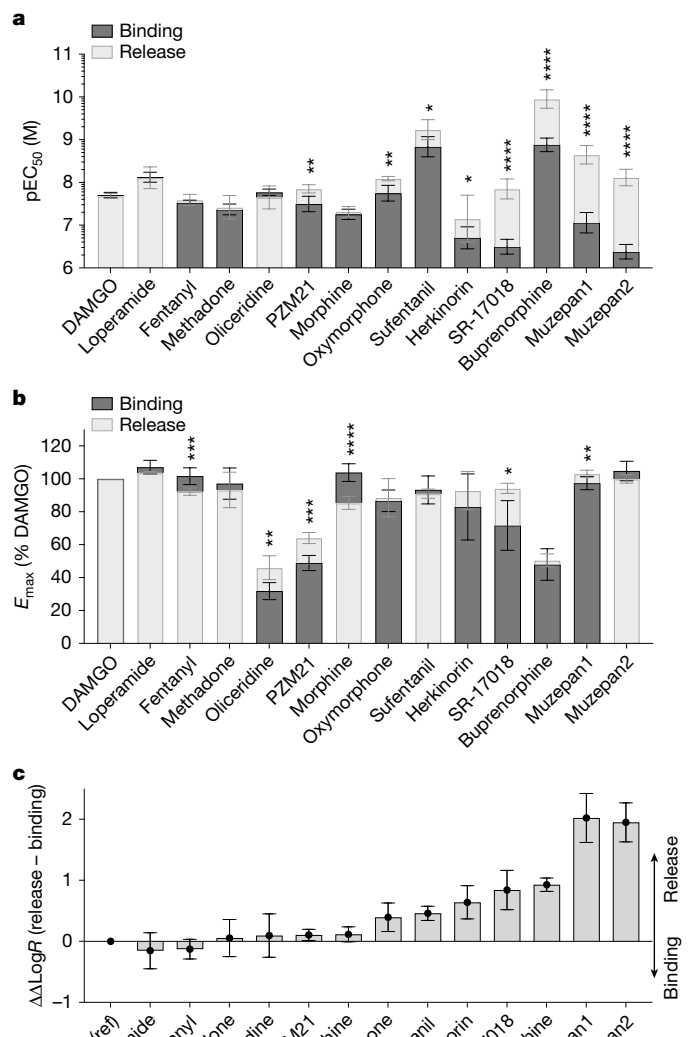


Fig. 2 | Opioid agonists exhibit differential preferences for GTP binding and release in CHO-MOR cell membranes. **a–c**, Comparisons of the mean of the individual ^{35}S -GTPyS binding and release: potencies (a), maximum efficacies (E_{\max}) normalized to DAMGO (100% versus baseline (0%)) (b), and difference in transduction efficiencies ($\Delta\Delta\log R$, relative to DAMGO) (c). Data are mean with 95% confidence interval. Unpaired *t*-test was used for comparing binding and release parameters for each compound. Extended Data Fig. 2 shows concentration–response curves and Extended Data Table 1 presents parameters and number of individual replicates ($n \geq 3$). **d**, Chemical structures of muzepan1 and muzepan2 with binding affinities (pK_i with s.e.m., $n = 6$; K_i is the inhibition constant) determined from competition binding assays with ^3H -naloxone.

membranes. In the binding experiment, DAMGO promotes only a 40% stimulation in the native tissue ((1.4 ± 0.01) -fold; $P < 0.001$, paired *t*-test versus baseline; Extended Data Fig. 4a). We determined that the sodium-free conditions lead to very high levels of GTPyS binding, making it difficult to see an effect of DAMGO on release. This is not unexpected, as there are relatively low levels of MOR in the system,

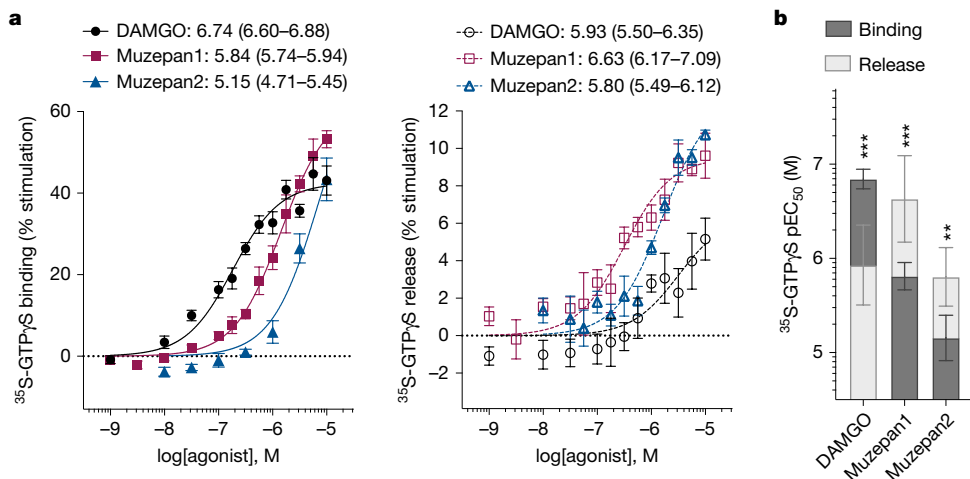


Fig. 3 | Bidirectional GTP exchange in mouse spinal cord membranes.

a, 35S -GTP γ S binding and release induced by indicated agonists. Data points show mean \pm s.e.m.; potencies are presented as pEC $_{50}$ with 95% confidence interval. Binding: DAMGO: $n = 8$; muzepan1: $n = 12$; muzepan2: $n = 4$.

b, Comparison of potencies between the binding and release exchange function for each agonist shown in **a**. Data are mean with 95% confidence interval. Unpaired, two-tailed, *t*-test of the mean of individual experiments.

as reflected by the approximately 40% stimulation in the binding studies (Extended Data Fig. 4a). Therefore, to isolate the MOR-accessible G-protein pool, we used DAMGO in the presence of sodium and 35S -GTP γ S in the pulse phase and diluted 100-fold as part of the chase (Methods and ref. 14). We demonstrate that this is feasible in the CHO-mMOR cell line, where the potencies of DAMGO are similar to those in the sodium-free loading conditions, although the potency for the release function is slightly decreased (19 nM binding versus 43 nM release; $P < 0.05$, *t*-test; Extended Data Fig. 4b). In mouse spinal cord membranes, when 100 nM DAMGO is included in the pretreatment period, there is an increase of about 10% in 35S -GTP γ S loading ($P < 0.001$; paired *t*-test), but no change is evident in the spinal cord of MOR-knockout mice (Extended Data Fig. 4c). We therefore took this modest stimulation as representative of MOR-mediated GTP γ S loading in the mouse spinal cord.

In mouse spinal cord membranes, DAMGO is more potent in stimulating 35S -GTP γ S binding than muzepan1 and muzepan2, whereas all agonists are full agonists (Fig. 3a). In the release paradigm, DAMGO loses potency, whereas muzepan1 and muzepan2 gain potency (Fig. 3b). Notably, the efficacy obtained by muzepan1 and muzepan2 reach the 10% maximal effect anticipated in the pulse loading (Extended Data Fig. 4c). This is in contrast to DAMGO, which does not reach this plateau, suggesting that in spinal cord, the enkephalin-like agonist may be selective against release. No significant effects were observed in spinal cord membranes from MOR-knockout mice (Extended Data Fig. 4d); therefore, the effects are likely to be due to MOR activation.

In mice, muzepan1 and muzepan2 are brain penetrant as they can be detected in brain 1 h following intraperitoneal injection of 3 mg kg $^{-1}$ of compound (muzepan1: 463 \pm 83 nM, muzepan2: 493 \pm 187 nM, $n = 3$; Extended Data Fig. 5a). We therefore tested the compounds for antinociceptive efficacy in the hot plate and warm water tail immersion assays and compared them with morphine (Fig. 4a). The potencies determined by the effect at 1 hour correlate with their rank order potency in GTP γ S binding (as well as release), although we note that at higher doses, muzepan1 remains nearly maximally efficacious for the 4 h duration of the test (Fig. 4b). Notably, none of the agonists have effects in MOR-knockout mice (Fig. 4b,c; for morphine see ref. 24).

Since muzepan1 and muzepan2 promote GTP release more potently than GTP binding, we considered whether a sub-efficacious dose would alter responsiveness to conventional opioid analgesics. When co-administered with 12 mg kg $^{-1}$ morphine, a low dose of muzepan1

(3 mg kg $^{-1}$) enhances and prolongs morphine-induced antinociception, and exceeds the calculated additive individual effects of each drug in both nociceptive tests (Fig. 5a). Furthermore, the inclusion of muzepan1 at varying doses of morphine produces the same enhancement, significantly improving the potency (median effective dose (ED $_{50}$)) of morphine by about two-fold ($P < 0.0001$; Fig. 5b and Extended Data Fig. 6) in both assays. Muzepan2 (12 mg kg $^{-1}$), which alone produces very little antinociception, also enhances and prolongs the response of morphine in a manner that is greater than additive (Fig. 5c).

To assure that the compounds are not indirectly enhancing morphine effects by competing with morphine metabolism, which occurs via glucuronidation 25 , we also used fentanyl, which is metabolized by CYP3A4 26 . Notably, neither compound competes with CYP3A4 as determined by *in vitro* competition studies (muzepan1: 11%, muzepan2: <10% inhibition at 10 μ M; Extended Data Fig. 5b). Whereas only male mice were tested with morphine owing to sex-dependent differences in morphine metabolism and sensitivity 27 , both male and female mice were tested with fentanyl, since the responses that we measured are comparable between the sexes 24,28 . When combined, muzepan1 dramatically prolongs the efficacy of fentanyl over time in a manner that is greater than the predicted additive effects of both compounds (Fig. 5d; see Extended Data Table 4 for statistical analyses of all time course data in Fig. 5).

Notably, the effects of muzepans on opioid-mediated antinociception resemble those of adding a positive allosteric modulator to an MOR agonist. Therefore, we tested whether muzepan1 could act allosterically by measuring its concentration-dependent effect on fentanyl-induced GTP γ S binding in spinal cord membranes. Since we do not observe a leftward shift in fentanyl potency, we cannot conclude that muzepan1 behaves as a positive allosteric modulator at MOR (Extended Data Fig. 7).

Whereas it is desirable to enhance the antinociceptive effects of analgesic opioids, it is not desirable to enhance the respiratory suppression and bradycardia associated with these agonists. Therefore, we tested the effect of muzepan1 alone and in combination with fentanyl in mouse pulse oximetry and heart rate monitoring studies (Fig. 6). Alone, muzepan1 produces respiratory suppression and bradycardia at 24 mg kg $^{-1}$ and 48 mg kg $^{-1}$ but not at 3 mg kg $^{-1}$; by contrast, fentanyl at lower doses (0.3 mg kg $^{-1}$ and 2 mg kg $^{-1}$) produces marked decreases in arterial oxygen saturation and heart rate (two-way repeated measures ANOVA, see Extended Data Table 5 for all comparisons). The response to the combination of 3 mg kg $^{-1}$ muzepan1

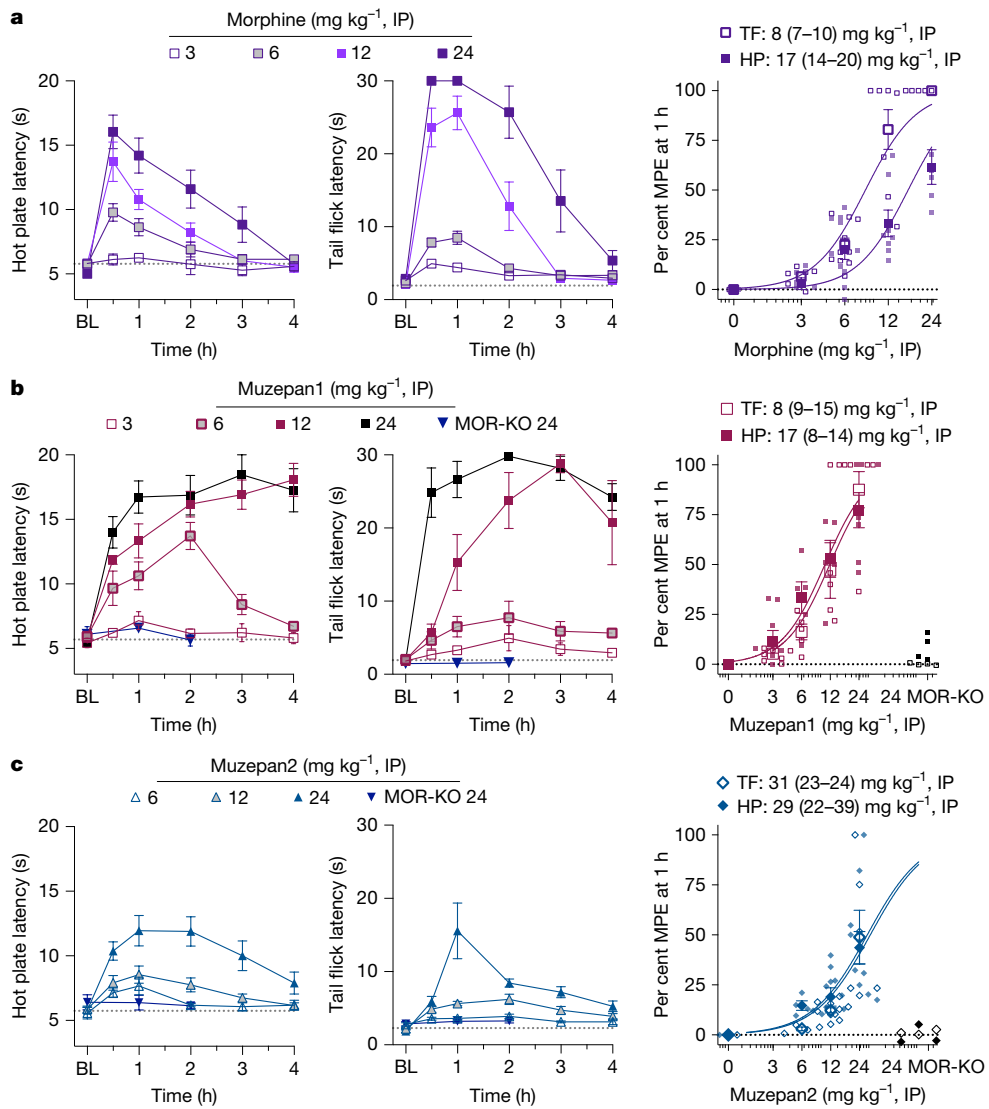


Fig. 4 | Potency in mouse hot plate and warm water tail immersion nociceptive assays. **a–c**, Morphine (a), Muzepan1 (b) and Muzepan2 (c) were tested at the indicated doses (in mg kg^{-1} , intraperitoneal injection (IP)) in the hot plate (left) and tail flick (middle) assays in wild-type and MOR-knockout (MOR-KO) mice. Right, potency was determined by comparing the response at 1 h based on the percentage of MPE calculated from the baseline (BL) and a cut-off time of 20 s for the hot plate and 30 s for the tail flick. Potency curves

are extended to convey 0% (determined by baseline) and 100% (determined by maximum cut-off time used to estimate the ED_{50}); potencies are presented with 95% confidence interval in the legends. **a**, Morphine: $n = 6$ (3 mg kg^{-1} and 24 mg kg^{-1}), $n = 10$ (6 mg kg^{-1} and 12 mg kg^{-1}). **b**, Muzepan1: $n = 8$ (3 mg kg^{-1}), $n = 5$ (6 mg kg^{-1} and 12 mg kg^{-1}), $n = 7$ (24 mg kg^{-1}); MOR-KO: $n = 5$. **c**, Muzepan2: $n = 4$ (6 mg kg^{-1}), $n = 10$ (12 mg kg^{-1}), $n = 6$ (24 mg kg^{-1}); MOR-KO: $n = 3$. HP, hot plate assay; TF, tail flick assay.

with 0.3 mg kg^{-1} or 2 mg kg^{-1} fentanyl does not differ from the effect produced by fentanyl alone in either assay. Furthermore, increasing the dose of muzepan1 to 24 mg kg^{-1} , a dose that produced mild but significant effects alone (two-way repeated measures ANOVA; Fig. 5 and Extended Data Table 5), is also not additive with fentanyl. Therefore, inclusion of muzepan1 with fentanyl prolongs fentanyl-induced antinociception, whereas respiratory and cardiac effects are not enhanced.

Discussion

The state-dependent interaction between GPCRs and G proteins that we reveal here implies an ongoing cycle that would affect the availability of the G proteins and their ability to engage with different effectors. Moreover, steric hindrance produced by a constitutive G-protein cycle may prevent the receptor from interacting with other effectors, particularly with direct binders, such as β -arrestins. It is

attractive to speculate that persistence of the cycle could prevent the recruitment of β -arrestins. This is consistent with the observation that many of the agonists that produce state-dependent increases in potency and/or efficacy of GTP release, have been characterized as G-protein-signalling-biased agonists (that is, those that are biased against recruiting β -arrestins). However, here we present compounds that diverge from this correlation. Specifically, we focus on two full agonists that do not show bias against β -arrestin recruitment, and demonstrate that the release state selectivity cannot be the only contributor to G-protein signalling bias. Although the exceptions can be identified, it remains possible that changes in the G-protein cycling kinetics will affect GPCR signalling bias.

Our study demonstrates that all opioid agonists tested in the transfected cell system promote GTP release and that the potencies for both release and binding are similar for many agonists. In mouse spinal cord membranes, agonists are less potent in the binding assays compared with in the transfected cell system; this is probably due to

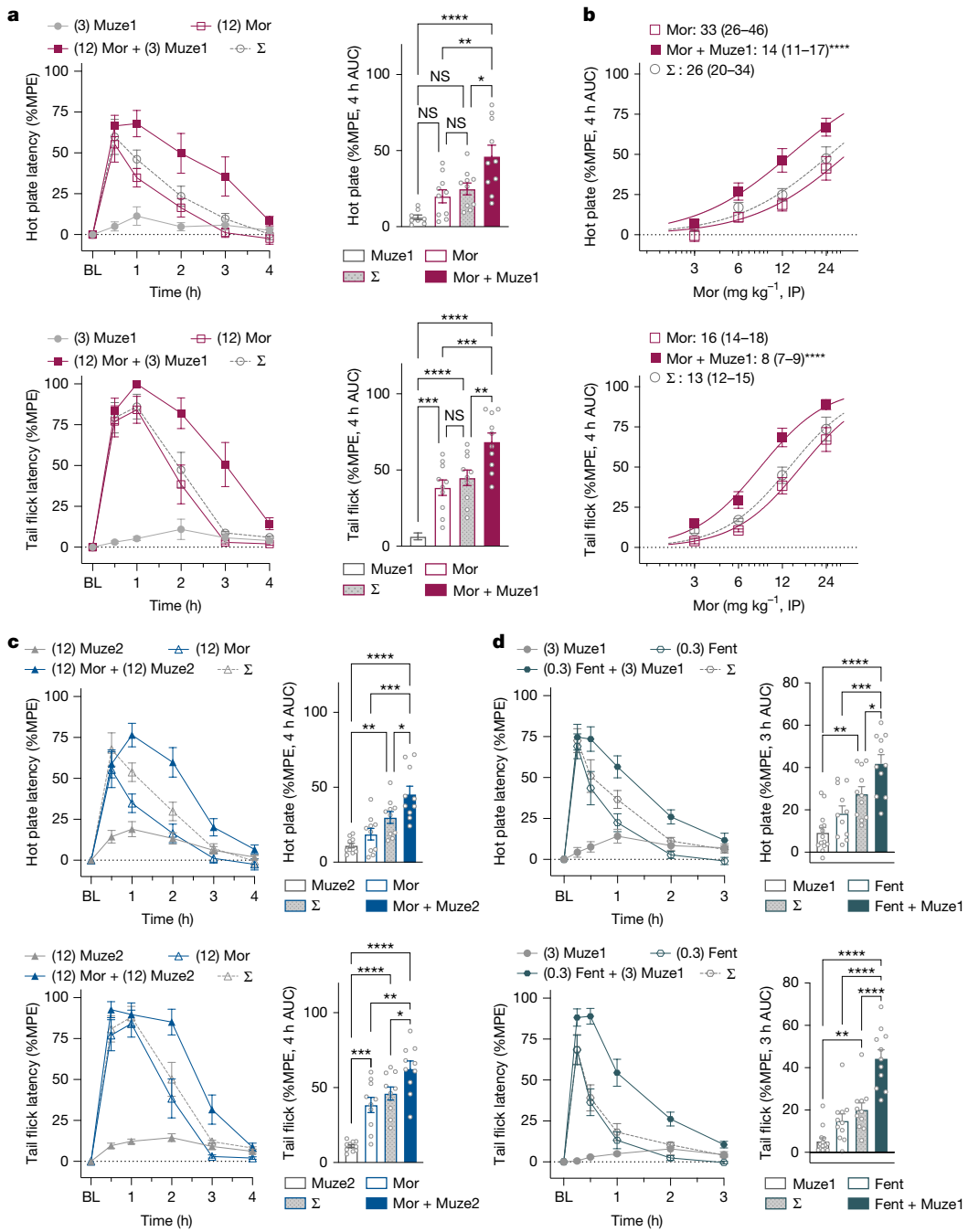


Fig. 5 | GTP-release-selective agonists enhance and prolong opioid-induced antinociception in mice. a, b. Hot plate (top) and tail flick (bottom) assays with muzepan1 (Muze1; 3 mg kg⁻¹, intraperitoneal) and morphine (Mor; 12 mg kg⁻¹, intraperitoneal) alone and combined. The calculated sum effect of both drugs (Σ) is shown for comparison. Right, mean (± s.e.m.) area under the curve (AUC). One-way ANOVA. **b, c, d.** AUC for 4 h hot plate (top) and tail flick (bottom) assays following treatment with different doses of morphine (Extended Data Fig. 6). Legend indicates the ED₅₀ (with 95% confidence interval). **c, d.** Muzepan2

(Muze2; 12 mg kg⁻¹, intraperitoneal) also enhances morphine (12 mg kg⁻¹, intraperitoneal)-induced antinociception (analysis as in a). **d**, Muzepan1 (3 mg kg⁻¹, intraperitoneal) prolongs fentanyl (Fent; 0.3 mg kg⁻¹)-induced antinociception in male and female mice (analysis as in a). See Extended Data Table 4 for two-way repeated measures ANOVA analyses of time course data for a–d and the number and sex of mice in each assay ($n = 6–14$; individual mouse data are shown as symbols in the bar charts) as well as the results of post hoc ANOVA analyses for drug effect over time.

the low representation of MOR-expressing neurons in the gross dissection of the spinal cord. In the same preparations, DAMGO-induced release is significantly diminished, and this decrease may be amplified by the low number of receptors in the preparation. Regardless of the concentration of receptor, the release induced by muzepons remains efficacious, and their potency is significantly improved, suggesting that the robust effect on release is preserved even in this heterogeneous endogenous system.

In this system, we have utilized a nonhydrolysable form of GTP (GTP γ S) to demonstrate that the GEF function of the GPCR is reversible and that agonists that show a preference for the reversal can have effects at sub-efficacious doses *in vivo*. It is important to acknowledge that, in the endogenous setting, we must consider that the GTP bound to the G protein is not stabilized and is still subject to hydrolysis by the intrinsic GTPase activity of the G protein. Further, this can be acted upon by other endogenous GAPs such as regulator of G-protein signalling

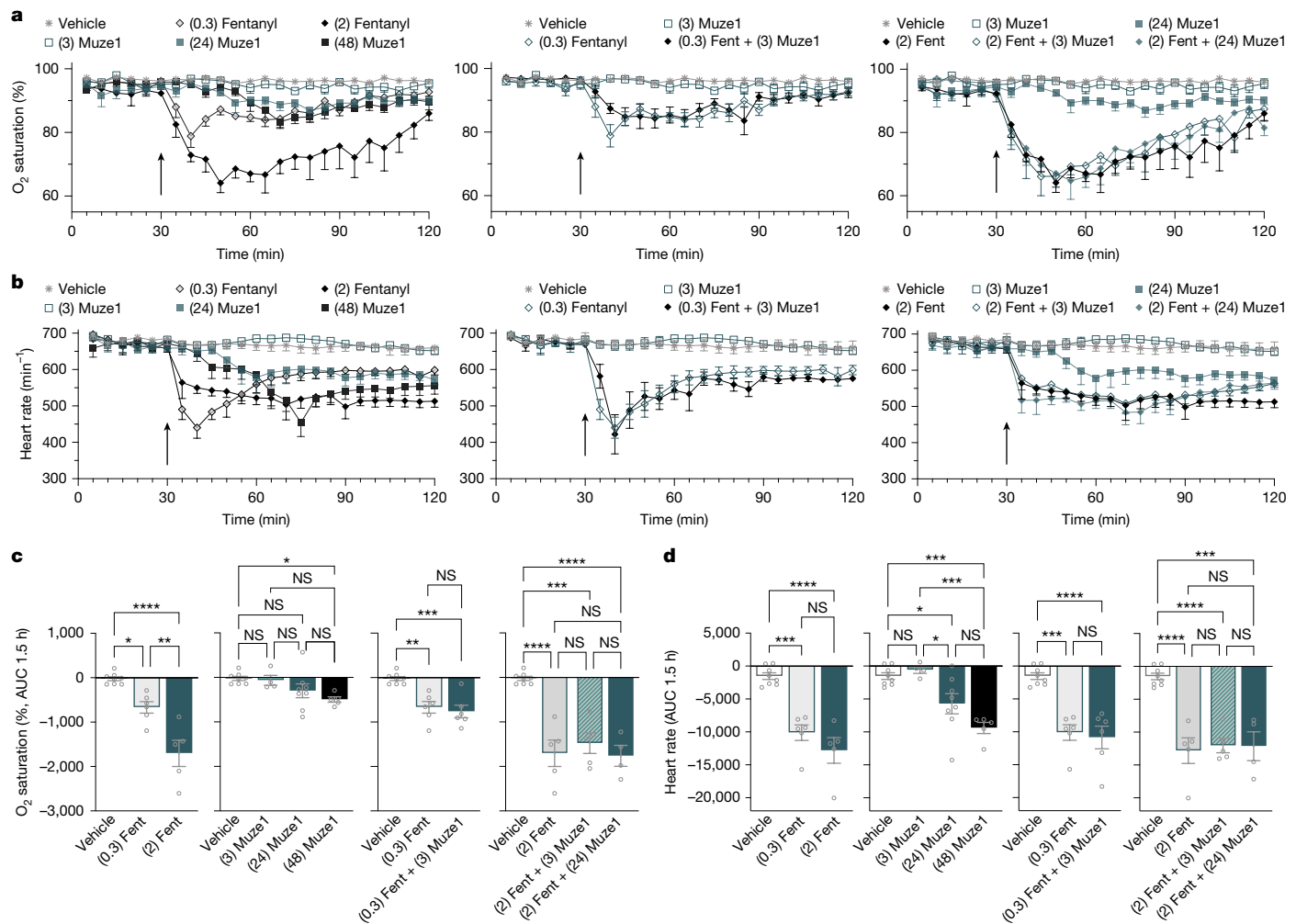


Fig. 6 | Muzepan1 does not enhance fentanyl-induced respiratory suppression or bradycardia in mice. a,b, Muzepan1 produces respiratory suppression (a) and bradycardia (b) at intraperitoneal doses of 24 mg kg⁻¹ and 48 mg kg⁻¹ but not at 3 mg kg⁻¹ in male and female mice. Neither dose alters fentanyl (0.3 mg kg⁻¹ or 2 mg kg⁻¹, intraperitoneal) effects when combined. **c,d**, The AUC for the 1.5 h after drug treatments (doses in mg kg⁻¹, intraperitoneal,

indicated in brackets) for oxygen saturation (c) and heart rate (d). One-way ANOVA with Tukey's post hoc test. See Extended Data Table 5 for two-way repeated measures ANOVA for time course data in a,b and number and sex of mice in each assay ($n = 4-8$; individual mouse data are shown as symbols in the bar charts).

(RGS) family proteins. However, if the receptor can promote GTP binding and release independent of the energy expenditure of hydrolysis, it may present a means to affect G-protein coupling kinetics which would change the effect of such GAPs in the system.

Our findings show that the receptor can facilitate GTP release; however, the context of the environment and the nature of the ligand will determine the ultimate consolidation of signalling. Therefore, the bidirectionality of the exchange function of a GPCR will affect the overall kinetics and energy landscape of GPCR activation. Thus, we propose a modification of the two-state model of receptor activation (as we present in Fig. 1a). We believe the net effect of an agonist on the fate of the G protein is a sum of the hydrolysis and the exchange, and not simply the forward reaction limited to energy-consuming hydrolysis.

The nature of the GTP_YS binding assay favours the detection of coupling to inhibitory G proteins owing to their abundance in cells; moreover, the actions at the MOR can be blocked by pertussis toxin, further implicating the $G\alpha_{i/o}$ class of proteins¹⁴. It remains to be determined whether this occurs for other G proteins (such as, G_s or G_q proteins). In addition to having a role in determining preference for G-protein signalling, the release cycle of one G protein could shift the preference of the receptor away from another G protein. Effectively, the release cycle of a previously coupled G protein would also compete with the

coupling of another class of G protein (that is, the inability to change coupling from G_i to G_q). One benefit of this approach is that it allows for the simultaneous assessment of two active states of the receptor in a single receptor population and that it can be amenable to testing in tissue. In the spinal cord, we note that DAMGO, an MOR-selective enkephalin analogue, is more potent in promoting GTP binding than release, whereas in the CHO overexpression cell lines, the DAMGO effects are nearly equivalent in both assays. Other GPCRs examined in the CHO cell lines may also prove to have differential affinities for one active state over the other when tested in the endogenous setting.

Our studies have shown that compounds that prefer the release state of the MOR are able to enhance and prolong the effects of opioid analgesics in mouse thermal nociception assays. We favour a model in which the receptor engages in multiple exchange events, keeping the G protein nearby to rapidly exchange nucleotide, and allowing another cycle to begin limiting the expenditure of energy through GTPase activity. This would enable the receptor-mediated G-protein activation to be reset without waiting for the completion of the GTPase cycle and, further, it keeps the proteins in close proximity. Of note, SR-17018 is also release-preferring, as well as a partial agonist, and a G-protein-signalling-biased agonist (over β -arrestin2 recruitment). In mice, it produces antinociception without respiratory suppression;

moreover, it does not lead to tolerance in several pain assays^{24,29,30}. In addition to being a G-protein-signalling-biased partial agonist, SR-17018 has also been shown to be a noncompetitive agonist that stabilizes G-protein signalling¹⁶. Moreover, treatment of morphine-tolerant mice with SR-17018 leads to a reversal of morphine tolerance while suppressing signs of withdrawal and restoring morphine sensitivity in mice²⁹. It is not yet clear what exact properties lead to SR-17018 restoration of sensitivity but the identification of this property and the further generation of probe compounds that preserve or eliminate each property independently will aid our studies to disentangle desirable opioid effects from unwanted side effects.

Notably, muzepan1 produces respiratory suppression and bradycardia at 24 and 48 mg kg⁻¹, which may not be unexpected, as it is a full agonist that does not show a preference for G-protein signalling over β-arrestin2 recruitment. However, whereas it is not surprising that the inactive dose of 3 mg kg⁻¹ muzepan1 does not produce an additive effect with 0.3 or 2 mg kg⁻¹ fentanyl, it is surprising that 24 mg kg⁻¹ dose of muzepan1, which alone does suppress activity, does not enhance or prolong the effects of 2 mg kg⁻¹ fentanyl on respiratory suppression or bradycardia. There remains the potential that we have reached a ceiling effect with the mice when combining the higher doses of each drug. However, we do note that the median lethal dose (LD₅₀) for fentanyl has been recorded at 113 mg kg⁻¹ (intraperitoneal) in C57BL/6 mice, suggesting that there should be potential to detect an additive decrease in oxygen saturation and heart rate³¹. Notably, the muzepans have been explored here for their robust ability to produce GTP release, and they may not be considered safer opioids at this time, as we clearly show that significant respiratory suppression can be observed with muzepan1 at high doses. Moreover, these probe compounds have not been evaluated for other opioid side effects, such as addiction liability, tolerance or dependence, nor have they been evaluated for general safety or toxicity. However, developing agonists that preserve the release preference, while also implementing other favourable properties, such as slow onset pharmacokinetics, partial agonism and fine-tuning preference for different signalling partners (β-arrestin versus G protein) is underway to improve the safety profile of such ligands.

With the examples provided here, we can conclude that at nearly inactive doses, muzepan1 enhances fentanyl-induced antinociception but does not enhance fentanyl-induced respiratory suppression in mice. We speculate that by favouring a release state of the receptor, either the receptor or the G proteins may have less opportunity to engage with secondary effectors that promote the cardiovascular side effects while perpetuating signalling that leads to antinociception. For example, a G protein that is cycling between GTP-bound and GDP-bound states may have more or fewer opportunities to interact with the Gβγ subunits, thereby preventing their further interaction with ion channels or other effectors, such as regulatory kinases or scaffolding proteins. Alternatively, the perpetual engagement between the receptor and G protein could sterically prevent engagement with other proteins, such as β-arrestins or other G-protein types. In this manner, one downstream signalling pathway may become more efficient while another is disengaged. In the case of SR-17018, a preference for promoting G-protein binding over β-arrestin2 recruitment as well as a preference over GIRK activation have been demonstrated^{24,32,33}. It remains to be determined what preferences will be desirable; however it is evident that the environment of the receptor in the tissue in which it mediates its response will dictate any preference for a secondary cascade.

By demonstrating that there are changes in both the rank order potency and efficacy of agonists, we demonstrate that there is a change in activity of the receptor for the GTP binding versus GTP release functions. Further, we conclude that the GTP binding and release events are independently regulated by receptor activity and that an agonist has the opportunity to not only promote G-protein activation but also to modulate G-protein activity in a state-selective manner. We demonstrate that a GTP-releasing agonist can enhance and prolong the

effects of conventional opioid agonists in antinociception without enhancing respiratory suppression or bradycardia in mice. Therefore, the selective modulation of potency and efficacy in the release function can change the dynamics of the drug effects in vivo. More broadly, since a ligand can induce a preference for exchange selectivity at a particular receptor, the agonist could thereby effectively regulate the availability of the Gα subunit for subsequent protein interactions and downstream signalling events. Overall, these findings demonstrate that for the opioid receptors, and possibly for all GPCRs, drug action will be a composite of its ability to promote both GTP binding and GTP release from the G protein.

Online content

Any methods, additional references, Nature Portfolio reporting summaries, source data, extended data, supplementary information, acknowledgements, peer review information; details of author contributions and competing interests; and statements of data and code availability are available at <https://doi.org/10.1038/s41586-025-09880-5>.

1. Helmreich, E. J. & Hofmann, K. P. Structure and function of proteins in G-protein-coupled signal transfer. *Biochim. Biophys. Acta* **1286**, 285–322 (1996).
2. Cassel, D. & Selinger, Z. Catecholamine-induced release of [³H]-Gpp(NH)p from turkey erythrocyte adenylate cyclase. *J. Cyclic Nucleotide Res.* **3**, 11–22 (1977).
3. Cassel, D., Levkovitz, H. & Selinger, Z. The regulatory GTPase cycle of turkey erythrocyte adenylate cyclase. *J. Cyclic Nucleotide Res.* **3**, 393–406 (1977).
4. Rodbell, M., Birnbaumer, L., Pohl, S. L. & Krans, H. M. The glucagon-sensitive adenyl cyclase system in plasma membranes of rat liver. V. An obligatory role of guanylnucleotides in glucagon action. *J. Biol. Chem.* **246**, 1877–1882 (1971).
5. Ross, E. M. & Gilman, A. G. Reconstitution of catecholamine-sensitive adenylate cyclase activity: interactions of solubilized components with receptor-replete membranes. *Proc. Natl. Acad. Sci. USA* **74**, 3715–3719 (1977).
6. Hildebrandt, J. D., Codina, J., Risinger, R. & Birnbaumer, L. Identification of a γ subunit associated with the adenylyl cyclase regulatory proteins N_γ and N_γ. *J. Biol. Chem.* **259**, 2039–2042 (1984).
7. Limbird, L. E., Gill, D. M. & Lefkowitz, R. J. Agonist-promoted coupling of the beta-adrenergic receptor with the guanine nucleotide regulatory protein of the adenylate cyclase system. *Proc. Natl. Acad. Sci. USA* **77**, 775–779 (1980).
8. Brandt, D. R. & Ross, E. M. Catecholamine-stimulated GTPase cycle. Multiple sites of regulation by beta-adrenergic receptor and Mg²⁺ studied in reconstituted receptor-G_α vesicles. *J. Biol. Chem.* **261**, 1656–1664 (1986).
9. Gilman, A. G. G proteins: transducers of receptor-generated signals. *Annu. Rev. Biochem.* **56**, 615–649 (1987).
10. Tolksdorf, A. M. & Levitzki, A. Coupling of a single adenylate cyclase to two receptors: adenosine and catecholamine. *Biochemistry* **17**, 3811–3817 (1978).
11. Bennett, N. & Dupont, Y. The G-protein of retinal rod outer segments (transducin). Mechanism of interaction with rhodopsin and nucleotides. *J. Biol. Chem.* **260**, 4156–4168 (1985).
12. May, D. C. & Ross, E. M. Rapid binding of guanosine 5'-O-(3-thiotriphosphate) to an apparent complex of beta-adrenergic receptor and the GTP-binding regulatory protein G_α. *Biochemistry* **27**, 4888–4893 (1988).
13. Traynor, J. R., Clark, M. J. & Remmers, A. E. Relationship between rate and extent of G protein activation: comparison between full and partial opioid agonists. *J. Pharmacol. Exp. Ther.* **300**, 157–161 (2002).
14. Bohn, L. M. & Stahl, E. L. Characterization of the GTP_S release function of a G protein-coupled receptor. *Nat. Commun.* <https://doi.org/10.1038/s41467-025-66516-y> (2025).
15. Asano, T. & Ross, E. M. Catecholamine-stimulated guanosine 5'-O-(3-thiotriphosphate) binding to the stimulatory GTP-binding protein of adenylate cyclase: kinetic analysis in reconstituted phospholipid vesicles. *Biochemistry* **23**, 5467–5471 (1984).
16. Stahl, E. L. et al. G protein signaling-biased mu opioid receptor agonists that produce sustained G protein activation are noncompetitive agonists. *Proc. Natl. Acad. Sci. USA* **118**, e2102178118 (2021).
17. Kenakin, T. & Christopoulos, A. Signalling bias in new drug discovery: detection, quantification and therapeutic impact. *Nat. Rev. Drug Discov.* **12**, 205–216 (2013).
18. DeWire, S. M. et al. A G protein-biased ligand at the mu-opioid receptor is potently analgesic with reduced gastrointestinal and respiratory dysfunction compared with morphine. *J. Pharmacol. Exp. Ther.* **344**, 708–717 (2013).
19. Manglik, A. et al. Structure-based discovery of opioid analgesics with reduced side effects. *Nature* **537**, 185–190 (2016).
20. Groer, C. E. et al. An opioid agonist that does not induce mu-opioid receptor-arrestin interactions or receptor internalization. *Mol. Pharmacol.* **71**, 549–557 (2007).
21. Ehrlich, A. T. et al. Biased signalling of the mu opioid receptor revealed in native neurons. *iScience* **14**, 47–57 (2019).
22. McPherson, J. et al. Mu-opioid receptors: correlation of agonist efficacy for signalling with ability to activate internalization. *Mol. Pharmacol.* **78**, 756–766 (2010).
23. Pedersen, M. F. et al. Biased agonism of clinically approved mu-opioid receptor agonists and TRV130 is not controlled by binding and signalling kinetics. *Neuropharmacology* **166**, 107718 (2020).
24. Schmid, C. L. et al. Bias factor and therapeutic window correlate to predict safer opioid analgesics. *Cell* **171**, 1165–1175.e1113 (2017).

25. Yeh, S. Y. Urinary excretion of morphine and its metabolites in morphine-dependent subjects. *J. Pharmacol. Exp. Ther.* **192**, 201–210 (1975).

26. Feierman, D. E. & Lasker, J. M. Metabolism of fentanyl, a synthetic opioid analgesic, by human liver microsomes. Role of CYP3A4. *Drug Metab. Dispos.* **24**, 932–939 (1996).

27. Gabel, F., Hovhannisyan, V., Andry, V. & Goumon, Y. Central metabolism as a potential origin of sex differences in morphine antinociception but not induction of antinociceptive tolerance in mice. *Br. J. Pharmacol.* **180**, 843–861 (2023).

28. Craft, R. M. Sex differences in opioid analgesia: “from mouse to man”. *Clin. J. Pain* **19**, 175–186 (2003).

29. Grim, T. W. et al. A G protein signaling-biased agonist at the mu-opioid receptor reverses morphine tolerance while preventing morphine withdrawal. *Neuropsychopharmacology* **45**, 416–425 (2020).

30. Pantouli, F. et al. Comparison of morphine, oxycodone and the biased MOR agonist SR-17018 for tolerance and efficacy in mouse models of pain. *Neuropharmacology* **185**, 108439 (2021).

31. Smith, M. A. et al. “Tranq-dope” overdose and mortality: lethality induced by fentanyl and xylazine. *Front. Pharmacol.* **14**, 1280289 (2023).

32. Gillis, A. et al. Low intrinsic efficacy for G protein activation can explain the improved side effect profiles of new opioid agonists. *Sci. Signal.* **13**, eaaz3140 (2020).

33. Stahl, E. L. & Bohn, L. M. Low intrinsic efficacy alone cannot explain the improved side effect profiles of new opioid agonists. *Biochemistry* **61**, 1923–1935 (2022).

Publisher's note Springer Nature remains neutral with regard to jurisdictional claims in published maps and institutional affiliations.



Open Access This article is licensed under a Creative Commons Attribution-NonCommercial-NoDerivatives 4.0 International License, which permits any non-commercial use, sharing, distribution and reproduction in any medium or format, as long as you give appropriate credit to the original author(s) and the source, provide a link to the Creative Commons licence, and indicate if you modified the licensed material. You do not have permission under this licence to share adapted material derived from this article or parts of it. The images or other third party material in this article are included in the article's Creative Commons licence, unless indicated otherwise in a credit line to the material. If material is not included in the article's Creative Commons licence and your intended use is not permitted by statutory regulation or exceeds the permitted use, you will need to obtain permission directly from the copyright holder. To view a copy of this licence, visit <http://creativecommons.org/licenses/by-nc-nd/4.0/>.

© The Author(s) 2025

Methods

Chemicals

Compounds were obtained from the following vendors: Sigma-Aldrich: oxymorphone (O-004-1ML), loperamide (1448005), methadone hydrochloride (M0267), morphine sulfate pentahydrate (M8777), sufentanil citrate (SML0535), herkinorin (5.08018.0001), buprenorphine (B9275), serotonin hydrochloride (H9523), carbachol (C4382), naloxone hydrochloride (N7758) and GDP (G7127). Cayman Chemical: PZM21 (20576-10), fentanyl citrate (22659) and GTP γ S (35098). DAMGO (11711) was from Tocris Bioscience. Oliceridine (TRV-130; 510256) was from MedKoo Biosciences. Dynorphin A 1-17 (3195) was from Fisher Scientific. Somatostatin-14 was custom synthesized by CPC Scientific. Met-enkephalin (30-0-10) was from American Peptide Company. SR-17018, muzepan1 and muzepan2 were made in house. ^{35}S -GTP γ S (NEG030H001MC) was from Revvity. ^3H -(-)naloxone was provided by the National Institute on Drug Abuse (NIDA) Drug Supply Program.

Animals

Male and female C57BL/6J (JAX:000664) and male MOR-KO (JAX:007559) mice were purchased from The Jackson Laboratory. MOR-KO mice were maintained by homozygous breeding. Mice were housed in groups of 2–5 and maintained on a 12 h:12 h light:dark cycle with food and water ad libitum. All adult mice were naive and at least ten weeks old prior to injection. For thermal antinociception tests, investigators were blinded to drugs and doses being administered. Mice were administered drugs intraperitoneally at a volume of 10 μl per g; for combinations of drugs, a single solution was prepared. All mice were used in accordance with the National Institutes of Health Guidelines for the Care and Use of Laboratory Animals with approval by The Herbert Wertheim UF Scripps Institute of Biomedical Technology and Innovation Animal Care and Use Committee.

Cell lines

Chinese Hamster Ovary (CHO-K1) cells were purchased from ATCC. Human MOR (hMOR), mouse MOR (mMOR) and human KOR (hKOR) cells have been described previously²⁴. For the other cell lines, receptor constructs were purchased from cDNA Resource Center including SST₂R (SSTR20TN00), 5-HT_{1A}R (5TR01ATN00) and M₂R (MAR020TN00). The SSTR₂R, 5-HT_{1A}R and M₂R cell lines were produced by electroporation of a pcDNA3.1 vector containing the N-terminally HA-tagged receptor into the parental cell line. A BD FACSAria3 flow cytometer was utilized to select for individual cells expressing receptor utilizing an anti-HA AlexaFluor 488 conjugate antibody (1:200). hMOR, hKOR, SST₂R, 5-HT_{1A}R and M₂R cell lines were maintained under geneticin selection (500 μg μl^{-1}). The mMOR cell line was maintained under puromycin selection (500 μg μl^{-1}). Cells were maintained in 1:1 DMEM:F12 media supplemented with 10% heat-inactivated fetal bovine serum (HI-FBS) at 37 °C with 5% CO₂. Prior to use in assays, cells were serum-starved for 30 min (hMOR, hKOR, 5-HT_{1A}R and M₂R) or 2 h (mMOR and SST₂R) then removed from the plate with 5 mM EDTA in PBS with a scraper. Pellets were rinsed with PBS and frozen in 1.5 ml tubes at -80 °C until use. All cell lines were verified to be mycoplasma-free by monthly testing.

^{35}S -GTP γ S binding and release

^{35}S -GTP γ S binding. ^{35}S -GTP γ S binding in cell lines was performed similarly as previously described^{16,24}. In brief, for CHO-hMOR cells, pellets were homogenized with a Potter-Elvehjem Teflon-on-glass Dounce homogenizer in homogenization buffer (10 mM Tris (pH 7.4), 100 mM NaCl, 1 mM EDTA) then pelleted (20,000g, 4 °C, 30 min). All other cell lines (CHO-mMOR, CHO-hKOR, CHO-hSST₂R, CHO-h5-HT_{1A}R and CHO-hM₂R) were homogenized in 10 mM Tris (pH 7.4), 1 mM EDTA. All reactions were performed with 0.1% DMSO and 0.1 nM ^{35}S -GTP γ S

(specific acitivity = 1,250 Ci mmol $^{-1}$; Revvity) in 50 mM Tris (pH 7.4), 100 mM NaCl, 5 mM MgCl₂, 1 mM EDTA with differing quantities of protein and GDP. For CHO-hMOR, CHO-mMOR and CHO-5-HT_{1A}R cells, 10 μg protein and 10 μM GDP was used. CHO-M₂R cell reactions were performed with 3 μg protein and 3 μM GDP. CHO-SST₂R cell reactions were performed with 10 μg protein and 20 μM GDP. CHO-hKOR cell reactions were performed with 15 μg protein and 3 μM GDP. Reactions were terminated by rapid filtration through GF/B filters with cold water after a 1 h incubation. Filters were punched into 96-well Opti-plates (Revvity) and dried overnight. Radioactivity was measured with 100 μl per well MicroScint-20 on a MicroBeta 2 (Revvity). For determination of bias between GTP γ S and β -arrestin2 recruitment, ^{35}S -GTP γ S binding was performed in CHO-hMOR cells exactly as described²⁴ and is shown in Extended Data Fig. 3a.

For ^{35}S -GTP γ S binding in C57BL/6J and MOR-KO spinal cord, tissue was homogenized via a Polytronic Tissue Tearor (BioSpec Products, 985370) and then a glass-on-glass Dounce homogenizer in homogenization buffer (10 mM Tris (pH 7.4), 1 mM EDTA). Homogenate was pulled through a 28G insulin needle before pelleting at 20,000g, 4 °C, 30 min. Reactions were performed with 10 μg , 10 μM GDP, 0.1% DMSO and 0.1 nM ^{35}S -GTP γ S and incubated for 1 h at 25 °C. Reactions were terminated as described above.

^{35}S -GTP γ S release in sodium-free conditions. Membranes were prepared in 10 mM Tris (pH 7.4), 1 mM EDTA as described for ^{35}S -GTP γ S binding in (10 mM Tris (pH 7.4), 1 mM EDTA). For ^{35}S -GTP γ S loading (the 'pulse') of CHO-hMOR, CHO-mMOR and CHO-5-HT_{1A}R cells, 1 mg of protein was incubated with 1 nM ^{35}S -GTP γ S and 10 μM GDP in 20 ml of 50 mM Tris (pH 7.4), 5 mM MgCl₂, 1 mM EDTA for 1 h at 25 °C. Identical conditions were used for CHO-SST₂R cells except GDP was increased to 20 μM . For CHO-M₂R cells, 0.3 mg of protein was incubated in the same conditions with 3 μM GDP. For CHO-hKOR cells, 1.5 mg of protein was incubated with 3 μM GDP. Release was performed by diluting tenfold into 50 mM Tris (pH 7.4), 100 mM NaCl, 5 mM MgCl₂, 1 mM EDTA supplemented with 1 μM cold GTP γ S and GDP corresponding to the receptor utilized. Release was performed for 1 h at 25 °C then terminated as described for ^{35}S -GTP γ S binding. See Supplementary Fig. 1 for a schematic.

^{35}S -GTP γ S release following 100 nM DAMGO-stimulated loading. For CHO-mMOR cells and C57BL/6J spinal cord studies relying on 100 nM DAMGO for loading, membranes were prepared as described for the sodium-free loading conditions. Then, 1 mg of protein was incubated with 1 nM ^{35}S -GTP γ S, 10 μM GDP, and 100 nM DAMGO in 2 ml of 50 mM Tris (pH 7.4), 100 mM NaCl, 5 mM MgCl₂, 1 mM EDTA for 1 h at 25 °C. Release was performed in large-volume 96-well plates with 10 μg protein, 10 μM GDP, 0.1% DMSO, at 2 ml final volume and incubated for 1 h at 25 °C. Reactions were terminated as described above for ^{35}S -GTP γ S binding. See Supplementary Fig. 2 for a schematic.

Radioligand binding. ^3H -(-)naloxone binding studies were performed as previously described¹⁶. Membranes were prepared via homogenization with a Polytronic Tissue Tearor then glass-on-glass Dounce homogenization in homogenization buffer (50 mM Tris (pH 7.4), 1 mM EDTA). Homogenate was pulled through a 28G insulin needle before pelleting at 20,000g, 4 °C, 30 min. Binding was performed with 10 μg membrane in 10 mM Tris (pH 7.4) containing 1% DMSO and approximately 2 nM ^3H -naloxone (1.50–2.04 nM; specific acitivity = 48.19 Ci mmol $^{-1}$) at a final volume of 200 μl . Reactions were incubated for 1 h at 25 °C then filtered through GF/B fiberglass filters with cold 10 mM Tris (pH 7.4) by rapid filtration over GF/B filters and washed with cold 10 mM Tris buffer. Filters were punched into white, 96-well OptiPlate and dried overnight. Radioactivity was quantified using 100 μl per well MicroScint-20 on a MicroBeta2. The K_d of ^3H -(-)naloxone determined by homologous competition in these studies is 0.83 (0.33–1.1) nM, $n = 6$.

β-arrestin2 recruitment. β-arrestin2 recruitment was performed as previously described²⁴. In brief, U2OS-β-arrestin2-hMOR PathHunter cells were plated at a density of 5,000 cells per well in a 384-well, white-walled assay plate in OptiMEM supplemented with 1% HI-FBS and incubated at 37 °C with 5% CO₂ for 16–20 h. Drug was prepared in PBS and cells were treated for 90 min at 37 °C. β-arrestin2 recruitment was determined using the PathHunter Detection Kit and luminescence was measured using a BioTek Synergy Neo2 multimode plate reader (BioTek).

Cytochrome P450 inhibition. Inhibition studies were carried out with 10 μM compound incubated with human liver microsomes and selective marker substrates (1A2, phenacetin demethylation to acetaminophen; 2C9, tolbutamide hydroxylation to hydroxytolbutamide; 2D6, bufuralol hydroxylation to 4'-hydroxybufuralol; 3A4, midazolam hydroxylation to 1'-hydroxymidazolam). After a 10 min incubation, the reaction was terminated and the percent inhibition was determined as previously described³⁴.

Antinociception

Thermal antinociception was performed as previously described²⁴. Prior to testing, mice were habituated to the testing room for 1 h. The tail flick test was determined as the amount of time until a mouse rapidly flicked its tail when placed 2–3 cm into a 49 °C water bath with a cut-off applied at 30 s. The hot plate test was measured using a 52 °C hot plate analgesia meter (Columbus Instruments) and forepaw or hindpaw licking or flicking were observed with a maximum latency of 20 s to prevent tissue damage.

Respiration and heart rate measures

Respiratory and heart rate parameters were simultaneously measured using the MouseOx Plus pulse oximeter (Starr Life Sciences) as previously described^{16,24}. Two days prior to testing, mice were shaved around the neck and habituated for 30 min to the collars and 50 ml conical tubes which were modified to restrain the mice. The following day, the mice were habituated to the collars and restraint for 30 min. On testing day, the basal vital signs of the mice were determined for 30 min then animals were injected and monitored for 90 min.

Pharmacokinetics

Male C57BL/6J mice were injected intraperitoneally with muzepan1 or muzepan2 at the doses indicated and blood was collected at indicated time points. Brains were collected following cervical dislocation, and snap frozen in liquid nitrogen. Samples were subjected to liquid chromatography (Shimadzu)–tandem mass spectrometry from AB Sciex. Pharmacokinetic parameters were calculated using a noncompartmental model²⁴ (Phoenix WinNonlin, Pharsight).

Data analysis

Concentration response studies were analysed by nonlinear regression analysis following normalization (baseline = 0 and maximum response = 100%). For all of the studies, we used the mean of the individual experiments to generate the potency (logEC₅₀) and efficacy (E_{max}) values as presented as pEC₅₀ with 95% confidence interval in the figures and graphs and as pEC₅₀ with s.e.m. in the table. Both potency and efficacy parameters were produced using three-parameter nonlinear regression with adaptation of the equation:

$$\text{Response} = \text{basal} + \frac{E_{\max} - \text{basal}}{10^{(\log EC_{50} - X)} + 1}$$

where X is the agonist concentration in log molar units and logEC₅₀ is agonist potency in log molar units. Statistical analyses comparing binding and release parameters, for each compound, was performed

by unpaired *t*-test. For the MOR studies, DAMGO was tested in parallel for all compounds and was used for normalization (baseline = 0, DAMGO at 10 μM = 100%). Statistical comparisons between binding and release parameters were performed by unpaired *t*-test comparing the individual parameters determined in each experiment; the number of replicates are indicated in the table.

In addition, a form of the operational model frequently applied to bias analysis was employed as the binding and release assays were considered independent measures of agonist activity^{17,35}. The equation takes the form:

$$\text{Response} = \text{basal} + \frac{E_{\max} - \text{basal}}{1 + \left(\frac{1 + 10^{(X + \log K)}}{10^{(\log R_{\text{reference}} + \Delta \log R)}} \right)^n}$$

where basal and E_{max} describe the system limits, and n defines the transducer slope. For the reference agonist DAMGO, logK and ΔlogR are held constant at zero. In this case, the logR_{reference} for the reference agonist reduces to the plogEC₅₀. For full test agonists the logR_{reference} is held constant, from the fit of the reference agonist, and the ΔlogR is permitted to float. The logK is held constant at zero for all full agonists. For partial test agonists, the logR_{reference} is again held constant and the ΔlogR and logK are permitted to float.

For the determination of the transduction efficiency, the ΔlogR was determined for each individual assay with DAMGO serving as the reference agonist. The ΔΔlogR was determined by unpaired *t*-test between the ΔlogR from the G-protein release assay and the ΔlogR of the G-protein binding assay. The same approach was used to determine the bias factor comparing the ΔlogR in G-protein binding versus the ΔlogR in β-arrestin2 recruitment in the CHO-hMOR cells.

In radioligand binding studies, naloxone competition was fit to the homologous (naloxone) or heterologous (muzepan1, muzepan2) competition equation:

$$\text{Binding} = \text{bottom} + \frac{B_{\max} \times [{}^3\text{H}-\text{naloxone}]}{[{}^3\text{H}-\text{naloxone}] + 10^{\log(X)} + K_{\text{naloxone}}}$$

where, for ³H-naloxone binding, 'bottom' and B_{max} are the non-specific and maximum binding, [³H-naloxone] is the radioligand concentration, K_{naloxone} is the naloxone equilibrium dissociation constant, and X is the cold naloxone concentration in molar units. For muzepan1 and muzepan2, competition data were fit to the heterologous competition equation:

$$\text{Binding} = \text{bottom} + \frac{\text{Top} - \text{bottom}}{1 + \frac{10^{\log(X)}}{K_i \left(1 + \frac{[{}^3\text{H}-\text{naloxone}]}{K_{\text{naloxone}}} \right)}}$$

where parameter definitions are shared between the two equations. In the heterologous competition equation, Top is the maximum observed binding, K_i is the molar affinity constant of the competitive ligand, and X is the concentration of the competitive ligand. Experiments were run together and both [³H-naloxone] and K_{naloxone} are held constant for the analysis.

Antinociception. A maximum possible effect (%MPE) was calculated as 100% × [(baseline response – test response)/(cut-off time – baseline response)]. For the determination of potency, the %MPE was compared at the 1 h time point by nonlinear regression analysis in GraphPad Prism (v.10.4), sharing the Hill slope and constraining the bottom to 0 and the top to 100%. For the comparison of morphine potency with and without muzepan1, the AUC was determined from the %MPE over the 4 h testing period; this was normalized to the maximum possible effect (the AUC if all points reached 100%) and fit the nonlinear regression

Article

analysis. Statistical comparisons of the $\log ED_{50}$ were made between two curves in Prism using an extra-sum-of-squares *F* test.

Respiration and heart rate. A two-way repeated measures ANOVA was used to compare drug effects (35–120 min) as a function of time and the results are presented in Extended Data Table 5. In addition, the AUC was determined by normalizing to the first 30 min of habituation for the following drug effect over 1 h. These values were then compared by one-way ANOVA comparing to vehicle with a Dunnett's post hoc test, or between drug treatments (fentanyl versus fentanyl plus 3 mg kg⁻¹ or 24 mg kg⁻¹ muzepan1; 3 groups, Tukey's post hoc test).

Reporting summary

Further information on research design is available in the Nature Portfolio Reporting Summary linked to this article.

Data availability

All data shown in graphs are provided as a Source Data file.

34. Li, X., Song, X., Kamenecka, T. M. & Cameron, M. D. Discovery of a highly selective CYP3A4 inhibitor suitable for reaction phenotyping studies and differentiation of CYP3A4 and CYP3A5. *Drug Metab. Dispos.* **40**, 1803–1809 (2012).

35. Stahl, E. L., Zhou, L., Ehlert, F. J. & Bohn, L. M. A novel method for analyzing extremely biased agonism at G protein-coupled receptors. *Mol. Pharmacol.* **87**, 866–877 (2015).

Acknowledgements We acknowledge Klaus-Peter Hofmann for critical and constructive discussion of our preliminary findings. Funding was provided by the National Institute on Drug Abuse/NIH to L.M.B. (DA038964), and L.M.B. and T.D.B. (DA033073). Pharmacokinetic data were collected using a mass spectrometer funded by NIH grant 1S10OD030332-01.

Author contributions L.M.B. and E.L.S. conceived and designed the studies, supervised the experiments, analysed data and wrote the manuscript. E.L.S. developed the experimental design for the in vitro studies and performed both in vivo and in vitro experiments. E.L.S. defined the models. E.L.S., M.A.S. and V.Q.D. performed the biochemistry experiments and contributed to analysis. L.M.B. developed the experimental design for the in vivo studies. M.A.S. and E.L.S. performed the animal studies with the assistance of L.M.B. and V.Q.D. for extensive blinding and drug preparation. M.D.C. provided the pharmacokinetic studies. T.D.B. and N.M.K. designed and synthesized SR-17018, muzepan1 and muzepan2.

Competing interests The University of Florida holds a patent on SR-17018 with L.M.B. and T.D.B. (US10751335B2) and has filed for patent protection of muzepan1 and muzepan2 (with L.M.B., N.M.K. and E.L.S.). The other authors declare no competing interests.

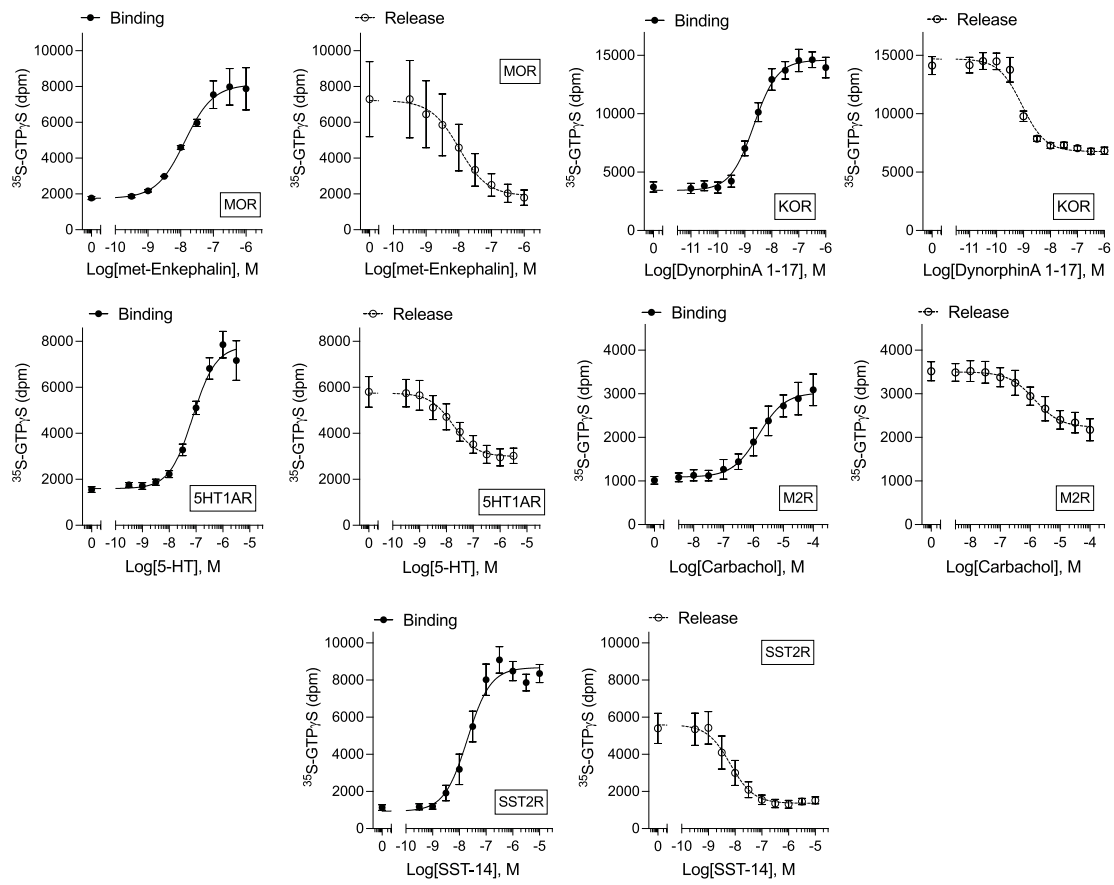
Additional information

Supplementary information The online version contains supplementary material available at <https://doi.org/10.1038/s41586-025-09880-5>.

Correspondence and requests for materials should be addressed to Edward L. Stahl or Laura M. Bohn.

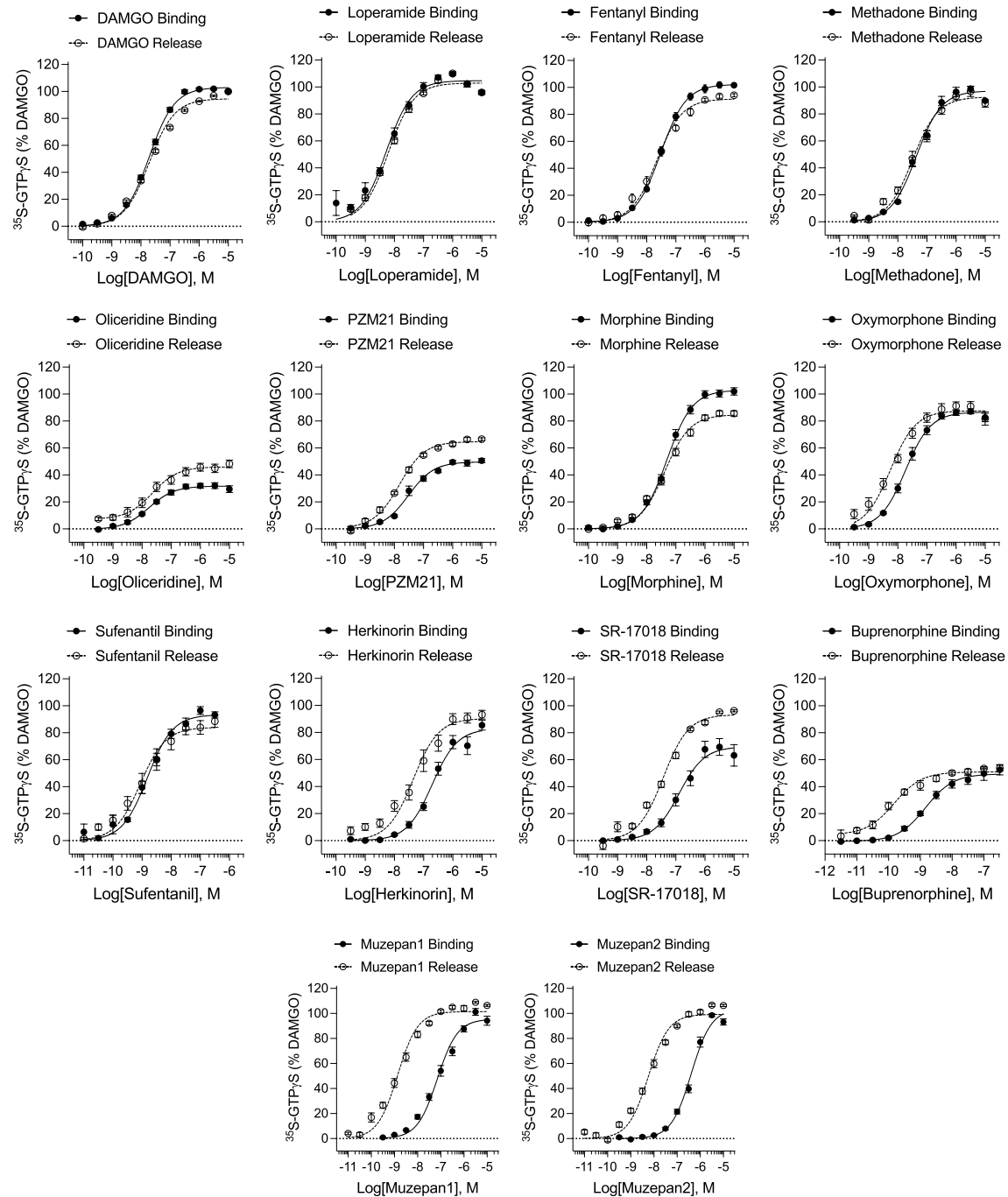
Peer review information *Nature* thanks Martin Lohse, Andrew Tobin and the other, anonymous, reviewer(s) for their contribution to the peer review of this work. Peer review reports are available.

Reprints and permissions information is available at <http://www.nature.com/reprints>.



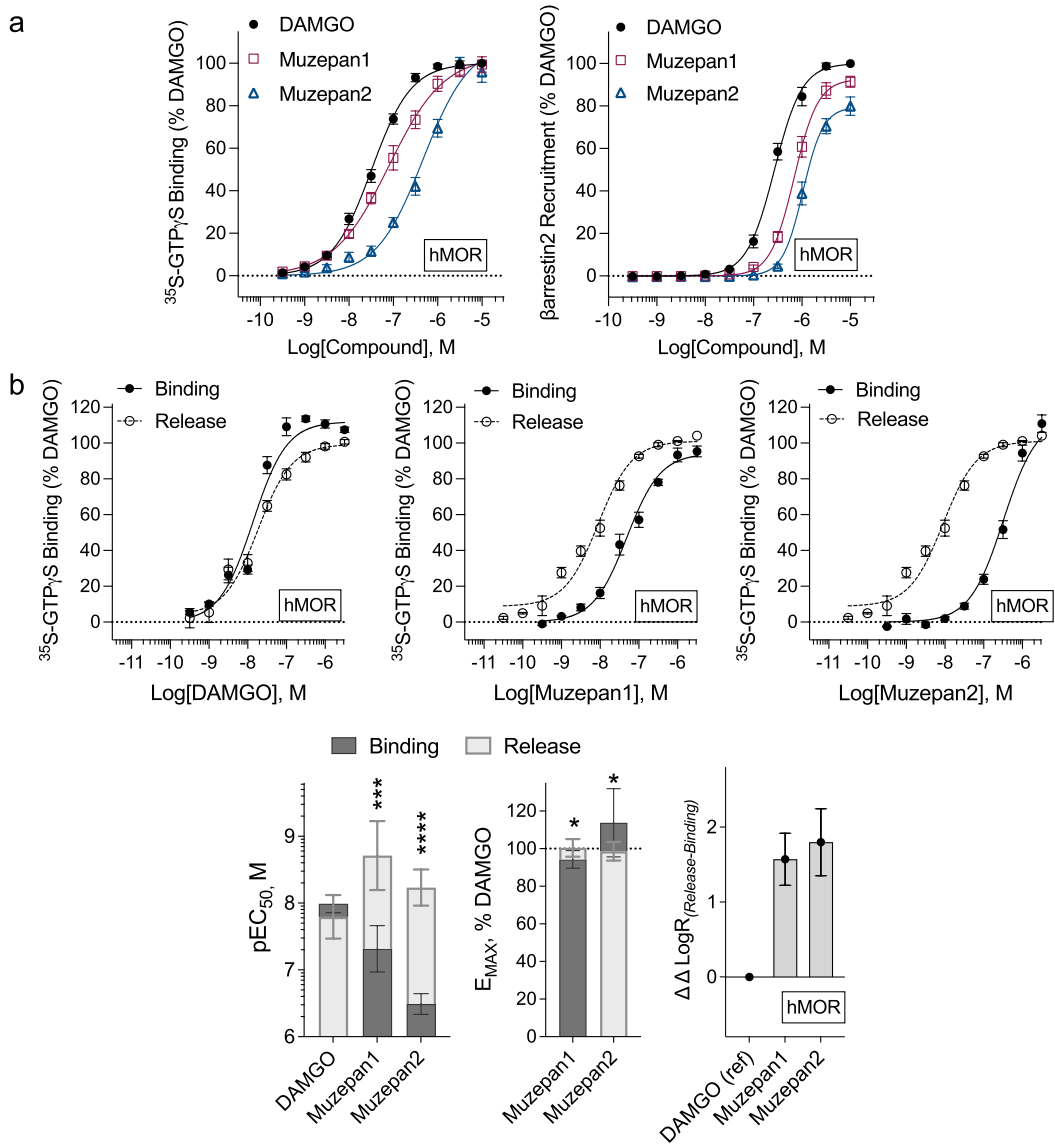
Extended Data Fig. 1 | GPCRs induce both GTP binding and release from $G\alpha_o$ proteins and the process is ligand dependent. Shown are the radioactivity counts (dpm) without normalization. Means with s.e.m are plotted, and the

parameters are presented with 95% CI in Fig. 1. MOR: n = 6 binding, 5 release; KOR: n = 3 binding, 5 release; 5HT1AR: 8 binding, 7 release; M2: n = 3 binding, 3 release; SST2: n = 4 binding, 4 release. Accompanies Fig. 1.



Extended Data Fig. 2 | Different opioid agonists show state selectivity for GTP binding or release. Shown are the responses to each agonist normalized to baseline (0%) and DAMGO max response (100%) assessed concurrently with a DAMGO concentration response curve. Means with s.e.m are plotted.

Accompanies Fig. 2 and Extended Data Table 1 which includes the number of replicates ($n \geq 3$) and curve parameters. DAMGO is the mean of all DAMGO run in parallel with each test opioid ($n = 56$ binding, $n = 45$ release).

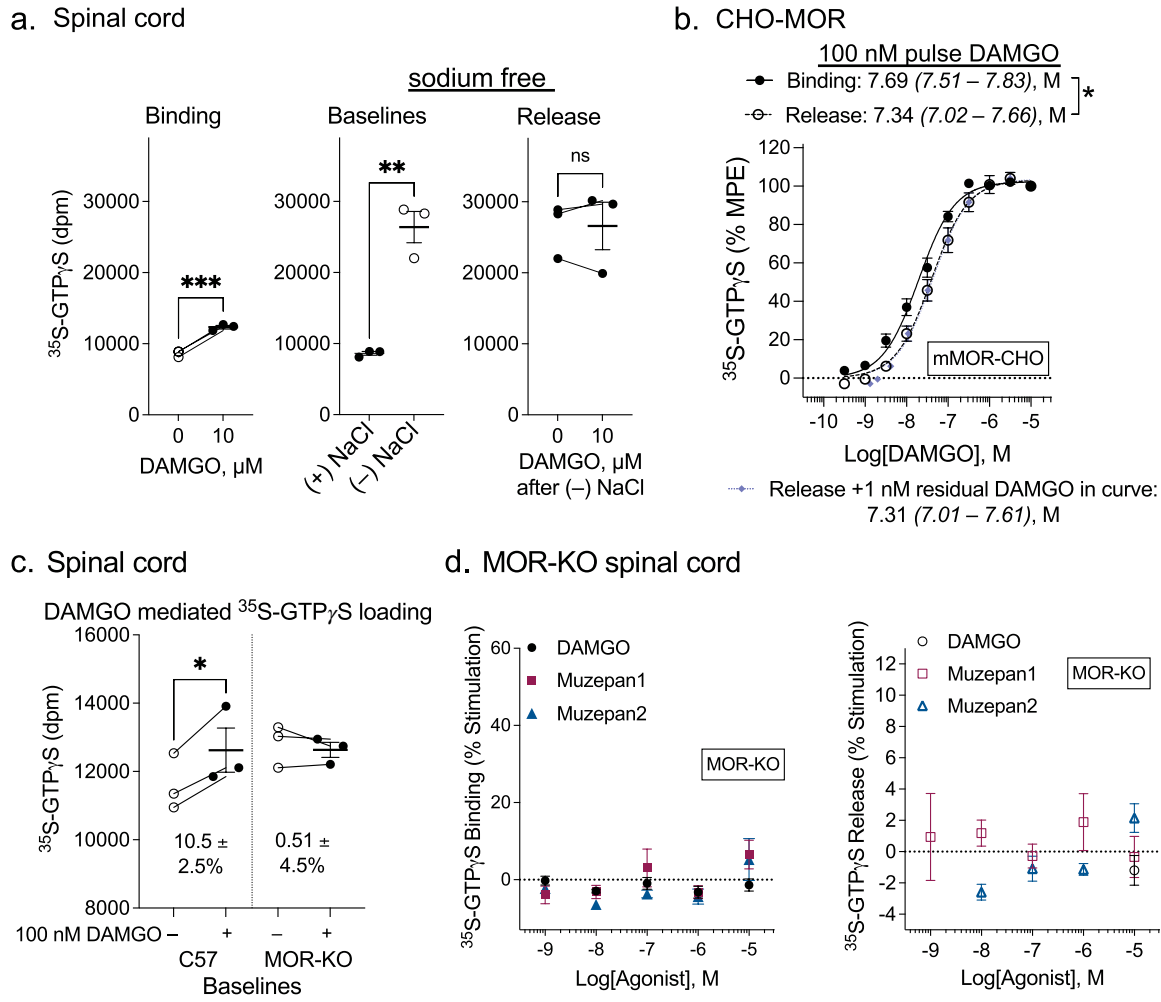


Extended Data Fig. 3 | Characterization of agonists at the human MOR.

a. Determination of GTP γ S binding in CHO-K1 cells expressing human MOR and β arrestin2 recruitment to the human MOR in U2OS PathHunter[®] cells from Millipore. See Extended Data Table 2 for EC₅₀, Emax and $\Delta\Delta\log R$ values with n.

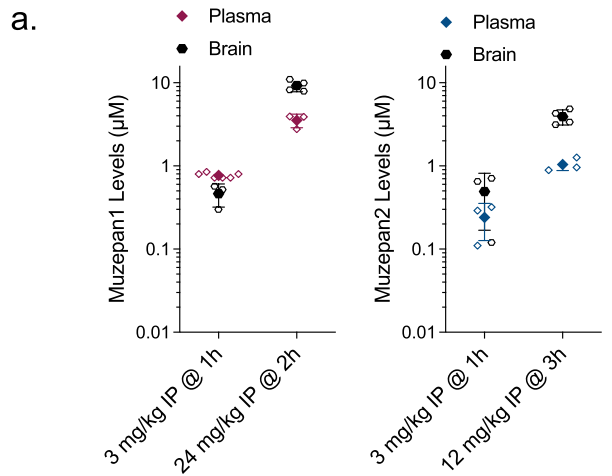
b. Comparison of GTP binding and release following sodium free loading of

³⁵S-GTP binding in hMOR CHO cell membranes with graphic presentation of the mean of the pEC₅₀ and Emax from individual experiments with 95% CI. The mean of the $\Delta\Delta\log R$ with 95% CI is presented and determined by comparing $\Delta\log R$ values from binding and release using an unpaired, two-tailed t-test. See Extended Data Table 3 for EC₅₀, Emax and presentation of $\Delta\Delta\log R$ with n.



Extended Data Fig. 4 | Adaptation of the method to spinal cord and verification in mMOR-CHO cells. **a.** Spinal cord from C57BL6/J male mice stimulated with 10 μ M DAMGO induces a 40% increase in GTP γ S binding over baseline (0) (left, $p < 0.001$, paired t-test, $n = 3$ mice as shown). Removing sodium from the system leads to an ~4-fold increase in baseline binding of ^{35}S -GTP γ S (middle, $**p < 0.01$, paired t-test, $n = 3$ mice). Under these conditions, DAMGO-induced release cannot be detected (right, $p > 0.05$ paired t-test, $n = 3$ mice). **b.** In CHO cells expressing mouse MOR cells, the inclusion of 100 nM DAMGO in the preloading condition, in the presence of sodium, is sufficient to

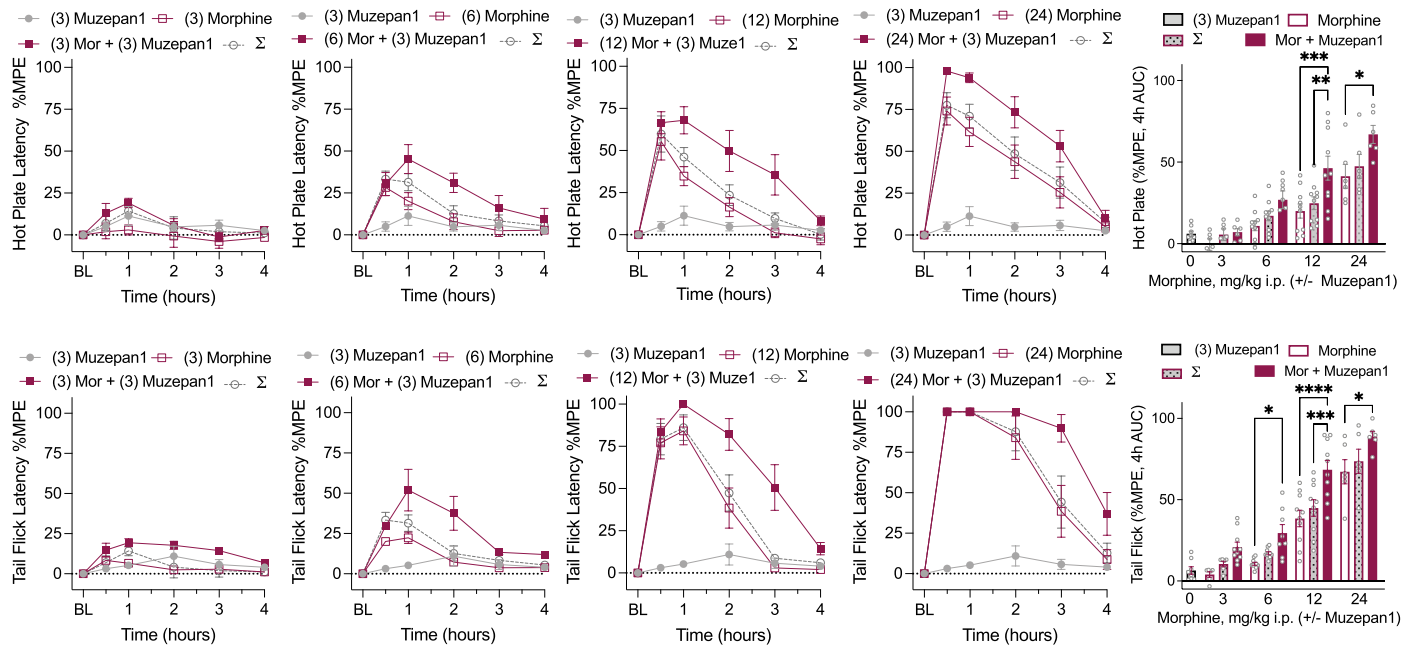
load the ^{35}S -GTP γ S and that DAMGO-mediated release can still be observed; the purple line and diamonds plots the curve with the consideration of the residual 1 nM remaining DAMGO in the chase (* $p < 0.05$ unpaired t-test comparing individual pEC_{50} ; pEC_{50} presented with 95%CI in figure legend). **c.** Use of 100 nM DAMGO in the preloading of spinal cord membranes results in a 10.5% increase in labeling that does not occur in membranes from MOR-KO mice (* $p < 0.05$ paired t-test, $n = 3$ mice). **d.** Neither ^{35}S -GTP γ S binding nor release is detected in spinal cord membranes from MOR-KO mice (plotted is the mean with s.e.m.; $n = 3$ mice per point). Accompanies Fig. 3.



b.

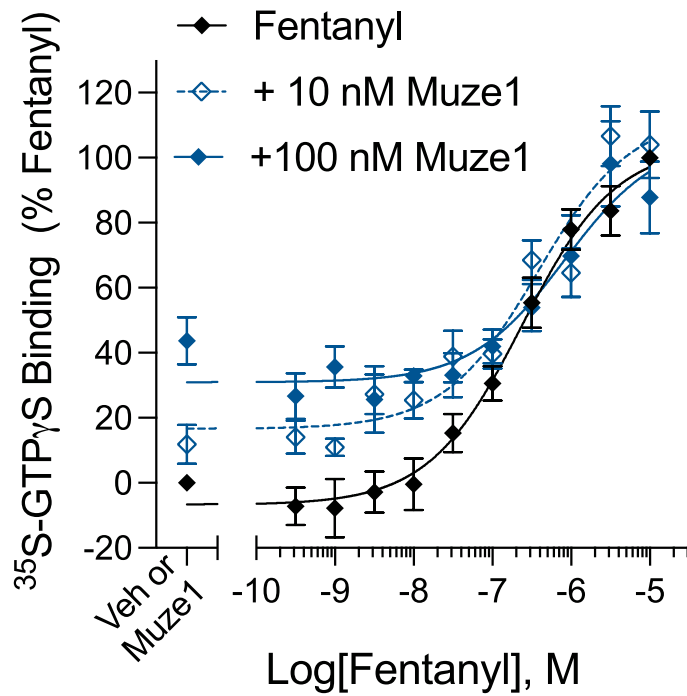
Compound ID	% inhibition at 10 μM unless noted			
	1A2	2C9	2D6	3A4
Furafylline (40 μM)	91	<10	<10	42
Sulfaphenazole	19	94	<10	40
Quinidine	<10	<10	90	<10
Ketoconazole (1 μM)	14	34	49	97
Muzepan1	<10	67	15	11
Muzepan2	<10	61	<10	<10

Extended Data Fig. 5 | Pharmacokinetic properties of Muzepan1 and Muzepan2. a. Brain and plasma levels measured in male C57BL6/J mice at the indicated time points; means with SD are shown (muzepan1: 3 mg/kg, n = 6 plasma, 3 brain; 24 mg/kg, n = 3 plasma, 4 brain; muzepan2: 3 mg/kg, n = 3 plasma, 3 brain; 24 mg/kg, n = 4 plasma, 4 brain). The conversion of tissue levels to molarity assumes 1 gram = 1 mL. b. Single point (10 μM) inhibition of cytochrome P450 enzymes presented as % inhibition and comparison to known standard inhibitors performed in duplicate.



Extended Data Fig. 6 | Hot plate (top) and Tail flick (bottom) responses of C57BL/6J male mice at indicated doses of morphine (mg/kg, i.p.) as indicated in the figure legends with 3 mg/kg i.p. Muzepan1. The sum of the mean effect of the two drugs is shown as Σ . Statistical comparisons over time are in Extended Data Table 2. Bar charts present the mean with s.e.m. of the area under the curve (AUC) calculated over the 4-hour assay. Statistical comparisons

are made by ordinary one-way ANOVA comparison within doses of morphine comparing morphine alone, the combination, and the calculated sum, * $p < 0.05$, *** $p < 0.001$, **** $p < 0.0001$. Mouse numbers are shown as circles in the AUC plots and also in Extended Data Table 4 along with 2-way RM-ANOVA comparing the effects over time with post-hoc analysis. Accompanies Fig. 5b.



Extended Data Fig. 7 | Competitive Schild analysis of fentanyl-stimulated GTP γ S binding in the presence of increasing concentrations of muzepan1 in mouse spinal cord. Data are normalized to 10 μ M point of fentanyl as 100% and to vehicle alone (0%). The potencies of fentanyl are shown in the table inset.

Muzepan1 alone is a full agonist, therefore, it stimulates binding at 10 and 100 nM when given alone (left x axis). Values for pEC_{50} and E_{max} are presented with 95% CI from analysis of the curves using GraphPad Prism (v. 10.4). ($n = 7$ individual mice with all three treatment groups assayed in parallel).

Article

Extended Data Table 1 | Pharmacological parameters from Fig. 2 presented as the mean pEC_{50} and E_{MAX} with s.e.m. determined from the mean of individual curves

mMOR	Binding				Release			
	pEC_{50} , M	E_{MAX}	$\Delta LogR$	n	pEC_{50} , M	E_{MAX}	$\Delta LogR$	n
DAMGO	7.71 \pm 0.032	100		56	7.68 \pm 0.029	100		45
Loperamide	8.12 \pm 0.046	107 \pm 2	0.5137 \pm 0.0554	6	8.11 \pm 0.059	104 \pm 0.2	0.3596 \pm 0.144	3
Fentanyl	7.52 \pm 0.028	102 \pm 2	-0.2364 \pm 0.0448	10	7.59 \pm 0.058	92 \pm 1	-0.1086 \pm 0.060	11
Methadone	7.37 \pm 0.029	97 \pm 2	-0.4931 \pm 0.0574	3	7.42 \pm 0.064	93 \pm 2	-0.4393 \pm 0.093	3
Oliceridine	7.77 \pm 0.030	32 \pm 2	-0.2186 \pm 0.0201	7	7.65 \pm 0.097	46 \pm 3	-0.0951 \pm 0.030	5
PZM21	7.50 \pm 0.056	49 \pm 1	-0.3643 \pm 0.0927	4	7.85 \pm 0.031	64 \pm 1	-0.2698 \pm 0.137	4
Morphine	7.25 \pm 0.057	104 \pm 3	-0.4532 \pm 0.0531	17	7.31 \pm 0.058	85 \pm 2	-0.3378 \pm 0.021	15
Oxymorphone	7.75 \pm 0.058	87 \pm 2	-0.1128 \pm 0.0573	4	8.09 \pm 0.016	89 \pm 4	0.2818 \pm 0.077	4
Sufentanil	8.83 \pm 0.091	93 \pm 3	0.8737 \pm 0.0514	6	9.23 \pm 0.091	91 \pm 1	1.3328 \pm 0.010	6
Herkinorin	6.71 \pm 0.060	83 \pm 5	-1.005 \pm 0.0091	3	7.15 \pm 0.127	93 \pm 3	-0.3652 \pm 0.098	3
SR-17018	6.50 \pm 0.074	72 \pm 6	-1.032 \pm 0.1029	8	7.85 \pm 0.073	94 \pm 1	-0.1915 \pm 0.080	4
Buprenorphine	8.88 \pm 0.065	48 \pm 4	0.7279 \pm 0.0343	7	9.95 \pm 0.084	51 \pm 1	1.6552 \pm 0.036	6
Muzepan1	7.06 \pm 0.098	97 \pm 2	-0.6882 \pm 0.1500	7	8.65 \pm 0.091	103 \pm 1	1.3331 \pm 0.113	8
Muzepan2	6.38 \pm 0.069	105 \pm 2	-1.308 \pm 0.1063	7	8.12 \pm 0.079	100 \pm 1	0.6414 \pm 0.101	7

The number of individual experiments is indicated (n). Accompanies Fig. 2 and Extended Data Fig. 2.

Extended Data Table 2 | Determination of GTP γ S binding in CHO-K1 cells expressing human MOR and β arrestin2 recruitment to the human MOR in U2OS PathHunter[®] cells from Millipore

hMOR	GTP γ S E _{MAX} (% DAMGO)	GTP γ S pEC ₅₀ , M	n	β arr2 E _{MAX} (% DAMGO)	β arr2 pEC ₅₀ , M	n	GTP γ S $\Delta\log R$	β arr2 $\Delta\log R$	$\Delta\Delta\log R$ (G – β)	95% CI
DAMGO	100	7.49 ± 0.021	7	100	6.57 ± 0.019	7				
Muzepan1	98 ± 2	7.10 ± 0.067	5	93 ± 2	6.16 ± 0.026	7	-0.3080 ± 0.0966	-0.4657 ± 0.0545	0.157	(-0.52 – 0.03)
Muzepan2	105 ± 3	6.33 ± 0.084	5	82 ± 2	5.98 ± 0.027	6	-1.043 ± 0.0217	-0.7936 ± 0.1104	-0.249	(-0.11 – 0.43)

See Extended Data Fig. 3b. Pharmacological parameters are presented as the mean pEC₅₀ E_{MAX} (% DAMGO max) and $\Delta\log R$ (DAMGO reference) with s.e.m. determined from the mean of individual curves with the number of replicates and error as indicated (n). The mean of the $\Delta\Delta\log R$ with 95% CI is presented and determined by comparing $\Delta\log R$ values from GTP binding and β arr2 recruitment using an unpaired, two-tailed t-test.

Article

Extended Data Table 3 | Determination of GTP binding and release in CHO-K1 cells expressing human MOR

hMOR	Binding				Release				$\Delta\Delta\log R$	
	pEC ₅₀ , M	E _{MAX}	$\Delta\log R$	n	pEC ₅₀ , M	E _{MAX}	$\Delta\log R$	n	(Rel-Bind)	(95% CI)
DAMGO	7.99 \pm 0.042	100		3	7.79 \pm 0.103	100		3		
Muzepan1	7.32 \pm 0.081	94 \pm 2	-0.706 \pm 0.079	3	8.71 \pm 0.120	100 \pm 1	0.887 \pm 0.118	3	1.57	(1.23 – 1.92)
Muzepan2	6.49 \pm 0.036	113 \pm 4	-1.291 \pm 0.059	3	8.23 \pm 0.063	99 \pm 1	0.465 \pm 0.133	3	1.72	(1.35 – 2.24)

Pharmacological parameters are presented as the mean pEC₅₀ and E_{MAX} (% DAMGO max) and $\Delta\log R$ (DAMGO reference) determined from the mean of individual curves with the number of replicates and error as indicated (n). The mean of the $\Delta\Delta\log R$ with 95% CI is presented and determined by comparing $\Delta\log R$ values from GTP binding and release using an unpaired, two-tailed t-test.

Extended Data Table 4 | Statistical analysis of the hot plate (HP) and tail flick (TF) studies as a function of dose and time presented in the indicated panels in Fig. 5

TIME COURSE over 4 hours									
Figure	Treatment	Compared to	Two-way RM ANOVA		P Value	F (DFn, DFd) drug effect	P Value	treatment n	Šídák's post-hoc time (h)
			F (DFn, DFd) time x drug	P Value					
HOT PLATE									
ED F 6	(3) Muzepan1	(3) Morphine	F (5, 60) = 0.6194	0.6855	F (1, 12) = 3.442	0.0883	8		
	(3) Morphine	(3) Morphine + Muzepan1	F (5, 50) = 1.711	0.1494	F (1, 10) = 4.447	0.0612	6	1*	
	SUM	(3) Morphine	F (5, 50) = 0.7125	0.6170	F (1, 10) = 1.804	0.2089	6		
	(3) Morphine + Muzepan1	SUM	F (5, 50) = 0.5348	0.7489	F (1, 10) = 0.3138	0.5877	6		
ED F 6	(3) Muzepan1	(6) Morphine	F (5, 80) = 4.564	0.0010	F (1, 16) = 3.255	0.0901	8	0.5**	
	(6) Morphine	(6) Morphine + Muzepan1	F (5, 80) = 3.237	0.0103	F (1, 16) = 6.314	0.0231	10	2*	
	SUM	(6) Morphine	F (5, 90) = 0.6902	0.6321	F (1, 18) = 2.127	0.1619	10		
	(6) Morphine + Muzepan1	SUM	F (5, 80) = 1.894	0.1045	F (1, 16) = 2.128	0.1639	8		
Fig 5a, ED F 6	(3) Muzepan1	(12) Morphine	F (5, 80) = 11.52	<0.0001	F (1, 16) = 9.102	0.0082	8	0.5**	
	(12) Morphine	(12) Morphine + Muzepan1	F (5, 90) = 2.938	0.0167	F (1, 18) = 10.82	0.0041	10	1*	
	SUM	(12) Morphine	F (5, 90) = 0.3376	0.8889	F (1, 18) = 1.191	0.2895	10		
	(12) Morphine + Muzepan1	SUM	F (5, 90) = 1.697	0.1434	F (1, 18) = 5.412	0.0319	10		
ED F 6	(3) Muzepan1	(24) Morphine	F (5, 60) = 21.02	<0.0001	F (1, 12) = 36.03	<0.0001	8	0.5**, 1**	
	(24) Morphine	(24) Morphine + Muzepan1	F (5, 50) = 3.336	0.0112	F (1, 10) = 8.609	0.0149	6		
	SUM	(24) Morphine	F (5, 50) = 0.1671	0.9735	F (1, 10) = 0.3342	0.5760	6		
	(24) Morphine + Muzepan1	SUM	F (5, 50) = 2.285	0.0602	F (1, 10) = 5.787	0.0370	6		
TAIL FLICK									
ED F 6	(3) Muzepan1	(3) Morphine	F (5, 50) = 1.916	0.1049	F (1, 10) = 0.3525	0.1049	8		
	(3) Morphine	Morphine + Muzepan1	F (5, 50) = 4.656	0.0014	F (1, 10) = 19.44	0.0013	6	1*, 2**, 3*	
	SUM	(3) Morphine	F (5, 50) = 5.325	0.0005	F (1, 10) = 5.904	0.0355	6	2**	
	(3) Morphine + Muzepan1	SUM	F (5, 50) = 1.109	0.3674	F (1, 10) = 3.728	0.0823	6		
ED F 6	(3) Muzepan1	(6) Morphine	F (5, 80) = 8.830	<0.0001	F (1, 16) = 8.055	0.0119	8	0.5****, 1**	
	(6) Morphine	(6) Morphine + Muzepan1	F (5, 80) = 4.261	0.0017	F (1, 16) = 17.02	0.0008	10	0.5*, 3**	
	SUM	(6) Morphine	F (5, 90) = 1.858	0.1096	F (1, 18) = 18.06	0.0005	10	2***, 3**	
	(6) Morphine + Muzepan1	SUM	F (5, 80) = 2.615	0.0305	F (1, 16) = 7.547	0.0143	8		
Fig 5a, ED F 6	(3) Muzepan1	(12) Morphine	F (5, 80) = 25.53	<0.0001	F (1, 16) = 37.37	<0.0001	8	0.5***, 1***	
	(12) Morphine	(12) Morphine + Muzepan1	F (5, 90) = 4.307	0.0015	F (1, 18) = 13.92	0.0015	10	3*, 4*	
	SUM	(12) Morphine	F (5, 90) = 0.1333	0.9843	F (1, 18) = 0.4609	0.5058	10	3**, 4*	
	(12) Morphine + Muzepan1	SUM	F (5, 90) = 3.422	0.0071	F (1, 18) = 10.06	0.0053	10		
ED F 6	(3) Muzepan1	(24) Morphine	F (5, 60) = 33.11	<0.0001	F (1, 12) = 117.2	<0.0001	8	0.5****, 1****, 2**	
	(24) Morphine	(24) Morphine + Muzepan1	F (5, 50) = 4.130	0.0032	F (1, 10) = 7.572	0.0204	6		
	SUM	(24) Morphine	F (5, 50) = 0.0519	0.9982	F (1, 10) = 0.1041	0.7536	6		
	(24) Morphine + Muzepan1	SUM	F (5, 50) = 3.403	0.0101	F (1, 10) = 6.030	0.0339	6		
HOT PLATE									
Fig 5c	(12) Muzepan2	(12) Morphine	F (5, 90) = 8.894	<0.0001	F (1, 18) = 5.018	0.0379	10	2*	
	(12) Morphine	(12) Morphine + Muzepan2	F (5, 90) = 6.979	<0.0001	F (1, 18) = 12.10	0.0027	10	0.5*, 1**, 2**	
	SUM	(12) Morphine	F (5, 90) = 1.103	0.3647	F (1, 18) = 3.131	0.0938	10		
	(12) Morphine + Muzepan2	SUM	F (5, 50) = 3.403	0.0018	F (1, 18) = 3.722	0.0696	10		
TAIL FLICK									
Fig 5c	12 Muzepan2	(12) Morphine	F (5, 90) = 30.12	<0.0001	F (1, 18) = 37.71	<0.0001	10	0.5 **, 1 ***	
	(12) Morphine	(12) Morphine + Muzepan2	F (5, 90) = 4.568	0.0009	F (1, 18) = 9.493	0.0064	10	2*	
	SUM	(12) Morphine	F (5, 90) = 0.2489	0.9393	F (1, 18) = 1.645	0.2159	10	3****, 4***	
	(12) Morphine + Muzepan2	SUM	F (5, 90) = 3.4820	0.0064	F (1, 18) = 4.572	0.0465	10		
all males ↑									
TIME COURSE over 3 hours									
HOT PLATE									
Fig 5d	(3) Muzepan1	(0.3) Fentanyl	F (5, 115) = 31.52	<0.0001	F (1, 23) = 16.65	0.0005	6f 8m	0.25****, 0.5****	
	(0.3) Fentanyl	Fentanyl + Muzepan1	F (5, 100) = 4.036	0.0022	F (1, 20) = 11.01	0.0034	6f 5m	0.5**, 1***, 2*	
	SUM	(0.3) Fentanyl	F (5, 100) = 0.4858	0.7861	F (1, 20) = 1.746	0.2012	6f 5m		
	Fentanyl + Muzepan1	SUM	F (5, 100) = 2.017	0.0826	F (1, 20) = 4.259	0.0523	6f 5m	0.5*	
TAIL FLICK									
Fig 5d	(3) Muzepan1	(0.3) Fentanyl	F (5, 115) = 41.45	<0.0001	F (1, 23) = 26.97	<0.0001	6f 8m	0.25****, 0.5****	
	(0.3) Fentanyl	Fentanyl + Muzepan1	F (5, 100) = 9.982	<0.0001	F (1, 20) = 27.26	<0.0001	6f 5m	0.5*, 1***, 2***, 3**	
	SUM	(0.3) Fentanyl	F (5, 100) = 0.2108	0.9572	F (1, 20) = 0.5103	0.4833	6f 5m		
	Fentanyl + Muzepan1	SUM	F (5, 100) = 9.442	<0.0001	F (1, 20) = 20.48	0.0002	6f 5m	0.5****, 1****	

Two-way RM-ANOVA with Šídák's post-hoc analysis for individual time points presented. The number of animals in the treatment group are indicated in the table as n, where m=male, f=female mice. (ED F): Extended Data Figure, *p<0.05, **p<0.01, ***p<0.001, ****p<0.0001 Šídák's post-hoc test.

Article

Extended Data Table 5 | Statistical analysis of the respiratory (% arterial oxygen saturation, %O2) and heart rate (beats per minute) measures as a function of dose and time over 1.5h

TIMECOURSE over 1.5 hours		Two-way RM ANOVA					
Figure	Treatment	Compared to	F (DFn, DFd) time x drug	P Value	F (DFn, DFd) drug effect	P Value	treatment n
%O2							
Fig 6a	(3) Muzepan1	Vehicle	F (17, 168) = 1.204	0.2664	F (1, 10) = 2.214	0.1613	2m 2f
	(24) Muzepan1	Vehicle	F (17, 235) = 2.343	0.0025	F (1, 14) = 23.58	0.0003	4m 4f
	(48) Muzepan1	Vehicle	F (17, 185) = 6.433	<0.0001	F (1, 11) = 47.53	<0.0001	3m 2f
	(0.3) Fentanyl	Vehicle	F (17, 200) = 5.494	<0.0001	F (1, 12) = 53.65	<0.0001	4m 2f
	(2) Fentanyl	Vehicle	F (17, 186) = 6.287	<0.0001	F (1, 11) = 48.96	<0.0001	3m 2f
	(0.3) Fentanyl + (3) Muzeapan1	Vehicle	F (17, 203) = 4.428	<0.0001	F (1, 12) = 26.70	0.0002	4m 2f
	(0.3) Fentanyl + (3) Muzeapan1	(0.3) Fentanyl	F (17, 167) = 1.670	0.0528	F (1, 10) = 0.1379	0.7181	4m 2f
	(2) Fentanyl + (3) Muzeapan1	Vehicle	F (17, 183) = 9.999	<0.0001	F (1, 11) = 83.04	<0.0001	3m 2f
	(2) Fentanyl + (24) Muzeapan1	Vehicle	F (17, 166) = 8.764	<0.0001	F (1, 10) = 183.0	<0.0001	2m 2f
	(2) Fentanyl + (3) Muzeapan1	(2) Fentanyl	F (17, 133) = 1.027	0.4337	F (1, 8) = 0.2246	0.6482	3m 2f
	(2) Fentanyl + (24) Muzeapan1	(2) Fentanyl	F (17, 116) = 0.6221	0.6902	F (1, 7) = 0.1726	0.8687	2m 2f
	Vehicle						4m 4f
HEART RATE							
Fig 6b	(3) Muzepan1	Vehicle	F (17, 169) = 1.800	0.0315	F (1, 10) = 0.09181	0.7681	2m 2f
	(24) Muzepan1	Vehicle	F (17, 235) = 1.634	0.0569	F (1, 14) = 7.984	0.0135	4m 4f
	(48) Muzepan1	Vehicle	F (17, 185) = 6.670	<0.0001	F (1, 11) = 21.85	0.0007	3m 2f
	(0.3) Fentanyl	Vehicle	F (17, 201) = 16.41	<0.0001	F (1, 12) = 22.00	0.0005	4m 2f
	(2) Fentanyl	Vehicle	F (17, 186) = 1.208	0.2617	F (1, 11) = 36.32	<0.0001	3m 2f
	(0.3) Fentanyl + (3) Muzeapan1	Vehicle	F (17, 203) = 5.619	<0.0001	F (1, 12) = 24.35	0.0003	4m 2f
	(0.3) Fentanyl + (3) Muzeapan1	(0.3) Fentanyl	F (17, 168) = 1.711	0.0450	F (1, 10) = 0.2691	0.6152	4m 2f
	(2) Fentanyl + (3) Muzeapan1	Vehicle	F (17, 184) = 1.612	0.0646	F (1, 11) = 44.75	<0.0001	3m 2f
	(2) Fentanyl + (24) Muzeapan1	Vehicle	F (17, 169) = 4.071	<0.0001	F (1, 10) = 32.37	0.0002	2m 2f
	(2) Fentanyl + (3) Muzeapan1	(2) Fentanyl	F (17, 134) = 0.6237	0.9717	F (1, 8) = 0.5891	0.4648	3m 2f
	(2) Fentanyl + (24) Muzeapan1	(2) Fentanyl	F (17, 119) = 2.167	0.0083	F (1, 7) = 0.002366	0.9626	2m 2f
	Vehicle						4m 4f

Two-way RM-ANOVA analysis between indicated groups was performed using GraphPad Prism (V.10.4). Accompanies Fig. 6. The number of animals in the treatment group are indicated in the table as n, where m=male, f=female mice.

Reporting Summary

Nature Portfolio wishes to improve the reproducibility of the work that we publish. This form provides structure for consistency and transparency in reporting. For further information on Nature Portfolio policies, see our [Editorial Policies](#) and the [Editorial Policy Checklist](#).

Please do not complete any field with "not applicable" or n/a. Refer to the help text for what text to use if an item is not relevant to your study.
For final submission: please carefully check your responses for accuracy; you will not be able to make changes later.

Statistics

For all statistical analyses, confirm that the following items are present in the figure legend, table legend, main text, or Methods section.

n/a Confirmed

- The exact sample size (n) for each experimental group/condition, given as a discrete number and unit of measurement
- A statement on whether measurements were taken from distinct samples or whether the same sample was measured repeatedly
- The statistical test(s) used AND whether they are one- or two-sided
Only common tests should be described solely by name; describe more complex techniques in the Methods section.
- A description of all covariates tested
- A description of any assumptions or corrections, such as tests of normality and adjustment for multiple comparisons
- A full description of the statistical parameters including central tendency (e.g. means) or other basic estimates (e.g. regression coefficient) AND variation (e.g. standard deviation) or associated estimates of uncertainty (e.g. confidence intervals)
- For null hypothesis testing, the test statistic (e.g. F , t , r) with confidence intervals, effect sizes, degrees of freedom and P value noted
Give P values as exact values whenever suitable.
- For Bayesian analysis, information on the choice of priors and Markov chain Monte Carlo settings
- For hierarchical and complex designs, identification of the appropriate level for tests and full reporting of outcomes
- Estimates of effect sizes (e.g. Cohen's d , Pearson's r), indicating how they were calculated

Our web collection on [statistics for biologists](#) contains articles on many of the points above.

Software and code

Policy information about [availability of computer code](#)

Data collection

Data analysis

For manuscripts utilizing custom algorithms or software that are central to the research but not yet described in published literature, software must be made available to editors and reviewers. We strongly encourage code deposition in a community repository (e.g. GitHub). See the Nature Portfolio [guidelines for submitting code & software](#) for further information.

Data

Policy information about [availability of data](#)

All manuscripts must include a [data availability statement](#). This statement should provide the following information, where applicable:

- Accession codes, unique identifiers, or web links for publicly available datasets
- A description of any restrictions on data availability
- For clinical datasets or third party data, please ensure that the statement adheres to our [policy](#)

Research involving human participants, their data, or biological material

Policy information about studies with [human participants or human data](#). See also policy information about [sex, gender \(identity/presentation\), and sexual orientation](#) and [race, ethnicity and racism](#).

Reporting on sex and gender

Reporting on race, ethnicity, or other socially relevant groupings

Population characteristics

Recruitment

Ethics oversight

Note that full information on the approval of the study protocol must also be provided in the manuscript.

Field-specific reporting

Please select the one below that is the best fit for your research. If you are not sure, read the appropriate sections before making your selection.

Life sciences Behavioural & social sciences Ecological, evolutionary & environmental sciences

For a reference copy of the document with all sections, see nature.com/documents/nr-reporting-summary-flat.pdf

Life sciences study design

All studies must disclose on these points even when the disclosure is negative.

Sample size Sample size for mouse studies was determined by power analysis comparing the expected drug induced change effect and the error associated with vehicle and control test compound.

Data exclusions one mouse was eliminated from 4mg/kg fentanyl treatment due to a poor collar fit and unreliable data acquisition.

Replication biochemical studies were replicated by two individuals with some drugs repeated by 3 people; mouse studies were replicated by two.

Randomization All biochemical studies were performed with DAMGO controls in parallel but with different drug replicates on different days. In mice, different drugs and doses were randomly tested on different days to insure that dose effect was reproducible across days.

Blinding Experimenter was blinded to the dose and drug by another investigator and unblinding was performed after data entry.

Behavioural & social sciences study design

All studies must disclose on these points even when the disclosure is negative.

Study description

Research sample

Sampling strategy

Data collection

Timing

Data exclusions

Non-participation

Randomization

Ecological, evolutionary & environmental sciences study design

All studies must disclose on these points even when the disclosure is negative.

Study description

Research sample

Sampling strategy

Data collection

Timing and spatial scale

Data exclusions

Reproducibility

Randomization

Blinding

Did the study involve field work? Yes No

Field work, collection and transport

Field conditions

Location

Access & import/export

Disturbance

Reporting for specific materials, systems and methods

We require information from authors about some types of materials, experimental systems and methods used in many studies. Here, indicate whether each material, system or method listed is relevant to your study. If you are not sure if a list item applies to your research, read the appropriate section before selecting a response.

Materials & experimental systems

n/a	Involved in the study
<input type="checkbox"/>	<input type="checkbox"/> Antibodies
<input type="checkbox"/>	<input type="checkbox"/> Eukaryotic cell lines
<input type="checkbox"/>	<input type="checkbox"/> Palaeontology and archaeology
<input type="checkbox"/>	<input type="checkbox"/> Animals and other organisms
<input type="checkbox"/>	<input type="checkbox"/> Clinical data
<input type="checkbox"/>	<input type="checkbox"/> Dual use research of concern
<input type="checkbox"/>	<input type="checkbox"/> Plants

Methods

n/a	Involved in the study
<input type="checkbox"/>	<input type="checkbox"/> ChIP-seq
<input type="checkbox"/>	<input type="checkbox"/> Flow cytometry
<input type="checkbox"/>	<input type="checkbox"/> MRI-based neuroimaging

Antibodies

Antibodies used

Validation

Eukaryotic cell lines

Policy information about [cell lines and Sex and Gender in Research](#)

Cell line source(s)

Authentication

Mycoplasma contamination

Commonly misidentified lines
(See [ICLAC](#) register)

Palaeontology and Archaeology

Specimen provenance

Specimen deposition

Dating methods

Tick this box to confirm that the raw and calibrated dates are available in the paper or in Supplementary Information.

Ethics oversight

Note that full information on the approval of the study protocol must also be provided in the manuscript.

Animals and other research organisms

Policy information about [studies involving animals; ARRIVE guidelines](#) recommended for reporting animal research, and [Sex and Gender in Research](#)

Laboratory animals

Wild animals

Reporting on sex

Field-collected samples

Ethics oversight

Note that full information on the approval of the study protocol must also be provided in the manuscript.

Clinical data

Policy information about [clinical studies](#)

All manuscripts should comply with the ICMJE [guidelines for publication of clinical research](#) and a completed [CONSORT checklist](#) must be included with all submissions.

Clinical trial registration

Study protocol

Data collection

Outcomes

Dual use research of concern

Policy information about [dual use research of concern](#)

Hazards

Could the accidental, deliberate or reckless misuse of agents or technologies generated in the work, or the application of information presented in the manuscript, pose a threat to:

No	Yes
<input type="checkbox"/>	Public health
<input type="checkbox"/>	National security
<input type="checkbox"/>	Crops and/or livestock
<input type="checkbox"/>	Ecosystems
<input type="checkbox"/>	Any other significant area

Experiments of concern

Does the work involve any of these experiments of concern:

No	Yes
<input type="checkbox"/>	Demonstrate how to render a vaccine ineffective
<input type="checkbox"/>	Confer resistance to therapeutically useful antibiotics or antiviral agents
<input type="checkbox"/>	Enhance the virulence of a pathogen or render a nonpathogen virulent
<input type="checkbox"/>	Increase transmissibility of a pathogen
<input type="checkbox"/>	Alter the host range of a pathogen
<input type="checkbox"/>	Enable evasion of diagnostic/detection modalities
<input type="checkbox"/>	Enable the weaponization of a biological agent or toxin
<input type="checkbox"/>	Any other potentially harmful combination of experiments and agents

Plants

Seed stocks

Novel plant genotypes

Authentication

ChIP-seq

Data deposition

- Confirm that both raw and final processed data have been deposited in a public database such as [GEO](#).
- Confirm that you have deposited or provided access to graph files (e.g. BED files) for the called peaks.

Data access links

May remain private before publication.

Files in database submission

Genome browser session
(e.g. [UCSC](#))

Methodology

Replicates

Sequencing depth

Antibodies

Peak calling parameters

Data quality

Flow Cytometry

Plots

Confirm that:

- The axis labels state the marker and fluorochrome used (e.g. CD4-FITC).
- The axis scales are clearly visible. Include numbers along axes only for bottom left plot of group (a 'group' is an analysis of identical markers).
- All plots are contour plots with outliers or pseudocolor plots.
- A numerical value for number of cells or percentage (with statistics) is provided.

Methodology

Sample preparation

Instrument

Software

Cell population abundance

Gating strategy

- Tick this box to confirm that a figure exemplifying the gating strategy is provided in the Supplementary Information.

Magnetic resonance imaging

Experimental design

Design type

Design specifications

Behavioral performance measures

Imaging type(s)

Field strength

Sequence & imaging parameters

Area of acquisition

Diffusion MRI

Used

Not used

Preprocessing

Preprocessing software

Normalization

Normalization template

Noise and artifact removal

Volume censoring

Statistical modeling & inference

Model type and settings

Effect(s) tested

Specify type of analysis: Whole brain ROI-based Both

Statistic type for inference

(See [Eklund et al. 2016](#))

Correction

Models & analysis

n/a Involved in the study

- Functional and/or effective connectivity
- Graph analysis
- Multivariate modeling or predictive analysis

Functional and/or effective connectivity

Graph analysis

Multivariate modeling and predictive analysis

This checklist template is licensed under a Creative Commons Attribution 4.0 International License, which permits use, sharing, adaptation, distribution and reproduction in any medium or format, as long as you give appropriate credit to the original author(s) and the source, provide a link to the Creative Commons license, and indicate if changes were made. The images or other third party material in this article are included in the article's Creative Commons license, unless indicated otherwise in a credit line to the material. If material is not included in the article's Creative Commons license and your intended use is not permitted by statutory regulation or exceeds the permitted use, you will need to obtain permission directly from the copyright holder. To view a copy of this license, visit <http://creativecommons.org/licenses/by/4.0/>

